

UNCLASSIFIED

AD NUMBER
AD853711
NEW LIMITATION CHANGE
TO Approved for public release, distribution unlimited
FROM Distribution authorized to U.S. Gov't. agencies and their contractors; Critical Technology; APR 1969. Other requests shall be referred to Army Electronics Command, Fort Monmouth, NJ.
AUTHORITY
USAEC ltr, 27 Jul 1971

THIS PAGE IS UNCLASSIFIED

AD



Research and Development Technical Report
ECOM-0215-F

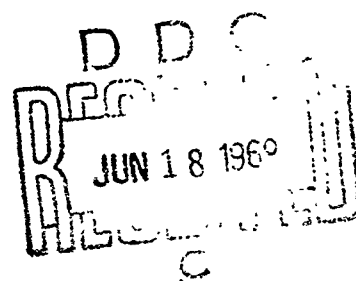
PULSED MAGNETIC FIELD FERROMAGNETIC
MICROWAVE GENERATOR

Final Progress Report

by

L.D. Buchmiller and F.A. Olson

April 1969



AD853711

ECOM

UNITED STATES ARMY ELECTRONICS COMMAND - FORT MONMOUTH, N.J.
Contract DAAB07-67-C-0215

MICROWAVE ELECTRONICS, A Teledyne Company, Palo Alto, California

DISTRIBUTION STATEMENT

This document is subject to special export controls and each transmittal to foreign governments or foreign nationals may be made only with prior approval of CG, U.S. Army Electronics Command, Fort Monmouth, New Jersey. Attn: AMSEL-KL-TG.

ACCESSION for	
CFS71	WHITE SECTION <input type="checkbox"/>
ORG	BUFF SECTION <input checked="" type="checkbox"/>
UNANNOUNCED	<input type="checkbox"/>
JUSTIFICATION	
BY	
DISTRIBUTION/AVAILABILITY CODES	
Dist.	Avail. and/or Special
2	

NOTICES

Disclaimers

The findings in this report are not to be construed as an official Department of the Army position, unless so designated by other authorized documents.

The citation of trade names and names of manufacturers in this report is not to be construed as official Government indorsement or approval of commercial products or services referenced herein.

Disposition

Destroy this report when it is no longer needed. Do not return it to the originator.

Technical Report ECOM-0215-F

Reports Control Symbol
OSD-1366
April 1969

PULSED MAGNETIC FIELD FERROMAGNETIC
MICROWAVE GENERATOR

Final Progress Report

Contract No. DAAB07-67-C-0215
DA Project No. 1H6-22001-A-055-05-06

Object

To develop a microwave nanosecond pulse generator
using ferrimagnetic materials subjected to pulsed
magnetic fields.

Prepared By

L.D. Buchmiller and F.A. Olson
MICROWAVE ELECTRONICS
Palo Alto, California

For

U.S. Army Electronics Command
Fort Monmouth, New Jersey 07703

DISTRIBUTION STATEMENT

This document is subject to special export controls and each transmittal to foreign governments or foreign nationals may be made only with prior approval of CG, U.S. Army Electronics Command, Fort Monmouth, New Jersey. Attn: AMSEL-KL-TG.

CONTENTS

	<u>Page</u>
ABSTRACT	iii
PART I: INTRODUCTION AND BACKGROUND	1
II. EXPLORATION INTO MULTI-SPHERE STRUCTURES	
A. Vane Structure	3
B. Loops in Cascade	3
C. Use of Strip Line Without Loops	7
III. DARLINGTON PULSER	19
IV. FEASIBILITY OF SOLID-STATE SWITCHES	
A. Introduction	21
B. Technical Considerations	21
1. Switch Specifications	22
2. Thyristors	22
3. P-I-N Diode	34
4. Glass Switch	36
C. Summary and Conclusions	36
V. X-BAND PULSED-FERRITE GENERATOR	
A. Generator Construction	39
1. X-Band Generator Chassis	39
B. RF Test Data	48
1. Q-Measurements	52
2. Tuning	54
3. RF Pulse Spectrum	54
4. Detected RF Pulse	54
5. Charged-Line Pulser Pulse Measurement	54
6. RF Power Output	59
VI. CONCLUSIONS	60
VII. REFERENCES	62

ILLUSTRATIONS

<u>Figure</u>	<u>Page</u>
1. The slotted loop, pulsed-field coil used in the prototype	4
2. (a) "Vane" periodic structure in rectangular waveguide; (b) Views of array of pulsed-field coils as a "vane" periodic traveling-wave structure.	5
3. Slotted pulsed-field coils in series with ungrounded conductor of pulsed-current strip line.	6
4. Same as Fig. 3, but with a common output waveguide.	8
5. Pieces of "cold-test hardware" representing three dif- ferent experiments.	10
6. Resonator cavity of short axial dimension (floating cylin- ders are supported by Styrofoam).	12
7. Waveguide with tiled half-wave resonator slots in the narrow wall.	13
8. Structure derived from a longitudinal slot (iris) in the ground side conductor of a slip line.	14
9. Structure of Fig. 8, disassembled. Iris and metal and dielectric parts of strip line are in the center.	15
10. Reflectometer oscillograms looking into structure of Figs. 8 and 9.	16
11. "Cold-test hardware" with strip line, irises and back-up cavities.	18
12. Leading edge of typical current pulse required by the pulsed ferrite microwave system.	23
13. Schematic of the thyristor and the equivalent two- transistor analog.	26
14. Illustration of the lateral spread of the "turned-on" region in an SCR.	27
15. Typical current increase during gate-triggering for an ideal SCR.	30
16. Schematic representation of the avalanche multiplication process in a reverse biased p-n junction.	33
17. Reverse voltage characteristic for a typical p-i-n diode.	36
18. Front view of the RF generator cabinet housing the pulsed ferrite X-band generator chassis (bottom) and the spark gap triggering circuit chassis (top).	41
19. Back view of the RF generator cabinet.	42
20. Pack view of the RF generator cabinet with the back cover removed.	43

ILLUSTRATIONS - CONTINUED

<u>Figure</u>	<u>Page</u>
21. Expanded view of the RF assembly and magnet shown in Fig. 2.	44
22. Top view of the RF generator chassis showing the spark gap video pulser, the trigger transformer and the RF assembly and its magnet.	46
23. Bottom view of the RF generator chassis.	48
24. Top view of the trigger chassis showing 100-volt power supply, charging choke and fan.	50
25. Bottom view of the trigger chassis.	51
26. Schematic circuit diagram of the over-all X-band pulsed-ferrite generator.	52
27. Plot of the measured value of the energy transfer-efficiency parameter versus frequency.	54
28. Tuning curve of the resonant slot versus tuning dial setting.	56
29. Photos of the spectrum of the 2 ns pulse RF output. The horizontal scale is 0.2 GHz/cm. The center frequency is 9.2 GHz.	57
30. Photo of the detected RF pulse as measured with 2.2 db attenuation. The horizontal scale is 1 ns/cm. The vertical scale is 50 mV/cm.	58
31. Photo of the charged line pulser voltage as measured on the output side of the sharpening gap.	59

ABSTRACT

Engineering and packaging improvements to a prototype X-band nanosecond pulsed-ferrite generator are described. Project effort has included:

- Investigations for increasing power output through the use of multiple ferrite sphere-resonator configurations.
- Improved charged-line spark-gap pulsers for providing pulsed magnetic fields for multiple-sphere configurations.
- Investigation of solid-state switch capabilities for replacing the spark-gap switches now required for switching the charged-line pulsers.
- Construction and testing of the final, triggered, X-band generator with a suitably compact form factor.

The final X-band pulsed ferrite generator uses a single YIG resonator and has the following features.

- Triggering of the spark-gap pulser with PRF's in the range to 600 pps is provided.
- The size of the charged-line pulser has been decreased by using a folded microstrip line construction.
- The generator is housed in a 16 x 21 x 24-inch cabinet.
- The generator is capable of delivering two-nanosecond RF pulses with less than one nanosecond risetime, and peak RF powers on the order of 150 watts in the X-band frequency range of 8 to 10 GHz.

PART I: INTRODUCTION AND BACKGROUND

The objective of this program is an engineering and packaging improvement of a prototype model, X-band, pulsed ferrite generator, based on the results achieved at Stanford University under Contract DA 28-043-AMC-00397(E).

The basic theory, final experimental model, and experimental results are described in a recent publication by Stanford personnel¹ and will not be repeated in this report.

The general purpose of the work was to determine the feasibility of a microwave generator in which a ferrite material is used to convert energy from a pulsed magnetic field into a coherent, X-band, pulsed RF energy.

The investigation includes studies of generator performance features and limitations, and the fabrication of an exploratory developmental model to demonstrate microwave generation of X-band power at nanosecond pulse widths by the use of a ferromagnetic material emersed in a pulsed magnetic field. The design objectives are as follows:

RF Pulse Width	1 to 3 nanoseconds
Center Frequency	9.6 GHz
Frequency Tuning Range	9.2 to 10.0 GHz
Peak Power	2 kW
Pulse Repetition Rate	1 to 10 KHz

The unit is to be self-contained, including triggered pulsing circuitry with only applied dc voltages required. Maximum over-all efficiency, reliability, life, and simplicity of operation are desired characteristics.

The principal efforts required were:

- determining methods of increasing power output,

- providing triggered pulse operation of the high current charged-line pulser, and
- constructing the deliverable developmental model in a suitably packaged form.

The principal methods considered for increasing power output were various configurations employing multiple-ferrite spheres. The multiple-sphere work was done chiefly on a subcontract basis with Stanford Research Institute (SRI) personnel* and was additionally supported by the consultant services of Dr. H.J. Shaw of Stanford University, who was responsible for the Stanford prototype model. The multiple-sphere work is described in Part II.

The final form of the recommended multiple-sphere configuration requires a 60 to 70 kV, 1.3 kA, 2ns pulser. Work on a Darlington charged-line pulser, which employs stepped characteristic impedance strip lines to obtain high pulse voltages for relatively low applied dc voltages, is described in Part III.

Other pulser considerations included a survey of solid-state switches to determine the future feasibility of replacing the spark-gap switches now employed in the pulser. This work was performed by D. Chambers of SRI and is described in Part IV.

A description of the construction and the RF test data of the X-band generator delivered on this contract is described in Part V. The generator uses a single YIG sphere since implementation of the multiple-sphere approach in the deliverable model proved to be beyond the scope of the program.

Conclusions are presented in Part VI.

*L. Young, A. Karp and D. Chambers.

II. EXPLORATION INTO MULTI-SPHERE STRUCTURES

The object is to augment the RF power output of the pulsed ferrite generator by increasing the number of YIG spheres in the system. Neglecting any interaction between spheres, the total power output would be proportional to the number of spheres, provided: (1) the same pulsed magnetic field is applied to all the spheres, and (2) the RF outputs from all the spheres can be coherently combined. Since each output pulse is brief in terms of the number of RF cycles contained, the tolerance on equality of the several output frequencies could be liberal--provided the starting phase was correct. Finding structures that can satisfy both provisions (1) and (2) has been difficult. Three of the various configurations considered are described below.

A. Vane Structure

The slotted loop, pulsed-field coil shown in Fig. 1 worked well in the single-sphere prototype generator¹. It was therefore originally proposed to increase the number of loops in parallel, from two upward and form a vane periodic structure as indicated in Fig. 2. The properties of this structure are well understood, and π -mode operation, with a YIG sphere in every other slot, appears the simplest. The reason this idea was dropped is the extreme difficulty of providing the very high pulse current needed to drive all the loops in parallel (typically 1500A per loop).

B. Loops in Cascade

Another method of using the original slotted loop pulsed-field coils that first appeared promising was to space them in series with the ungrounded conductor of the pulsed current strip line as shown in Fig. 3*. Individual waveguides

*In this report, the term "strip line" always refers to a two-conductor transmission line. The grounded conductor is often wider and thicker than the ungrounded conductor.

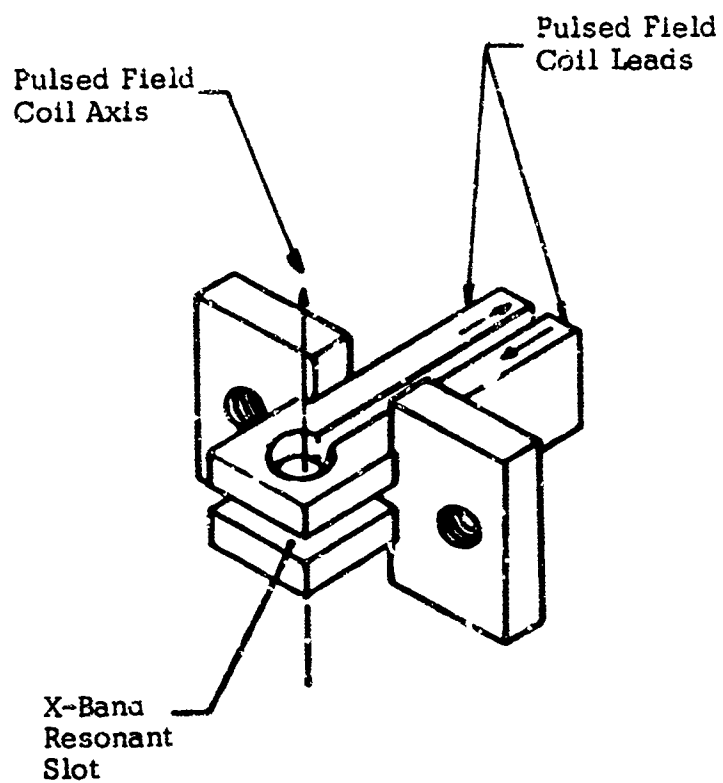


Fig. 1. The slotted loop, pulsed-field coil used in the prototype generator.

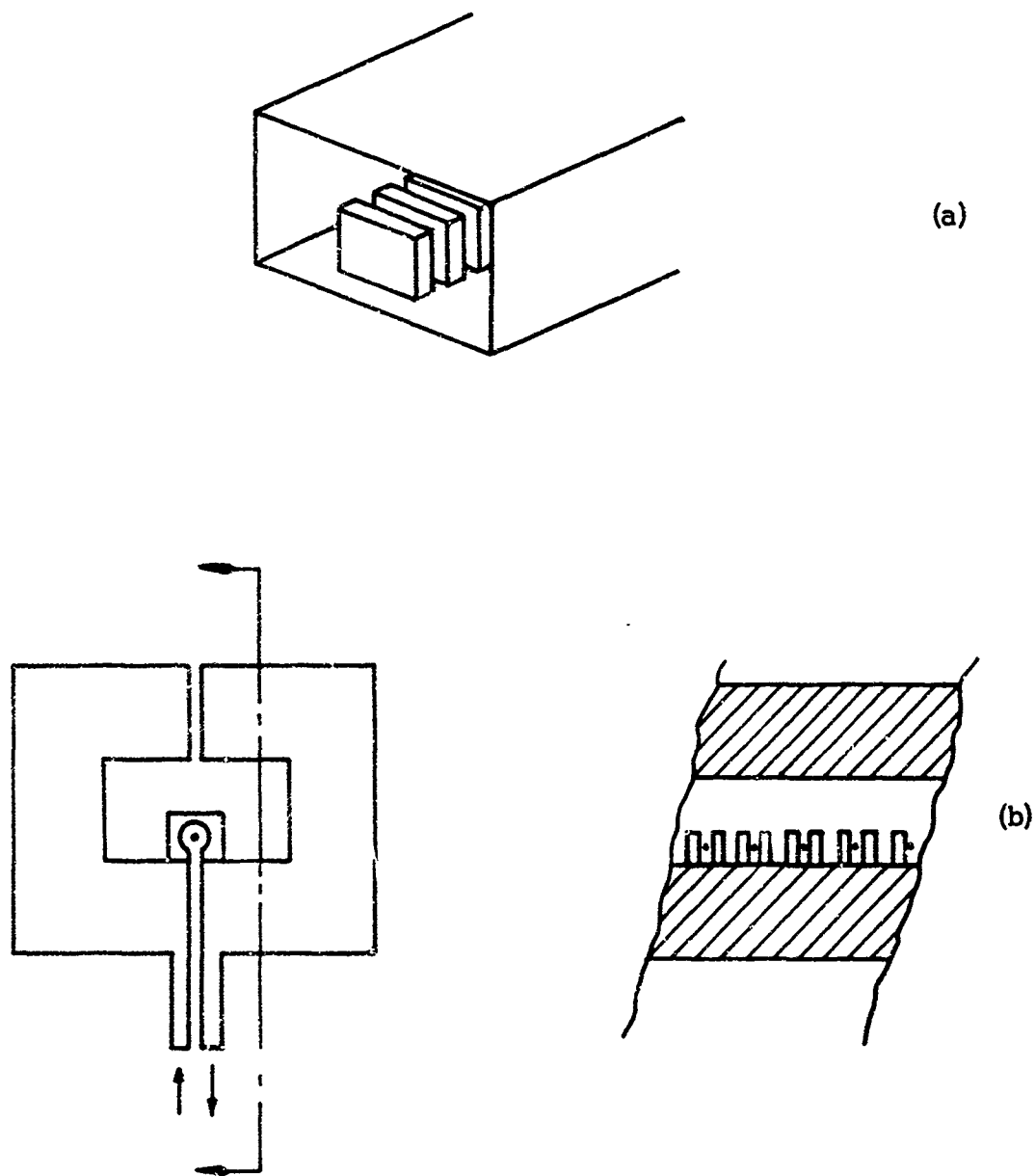


Fig. 2. (a) "Vane" periodic structure in rectangular waveguide;
 (b) Views of array of pulsed-field coils as a "vane" periodic
 traveling-wave structure. The solid circles represent the
 ferrite spheres.

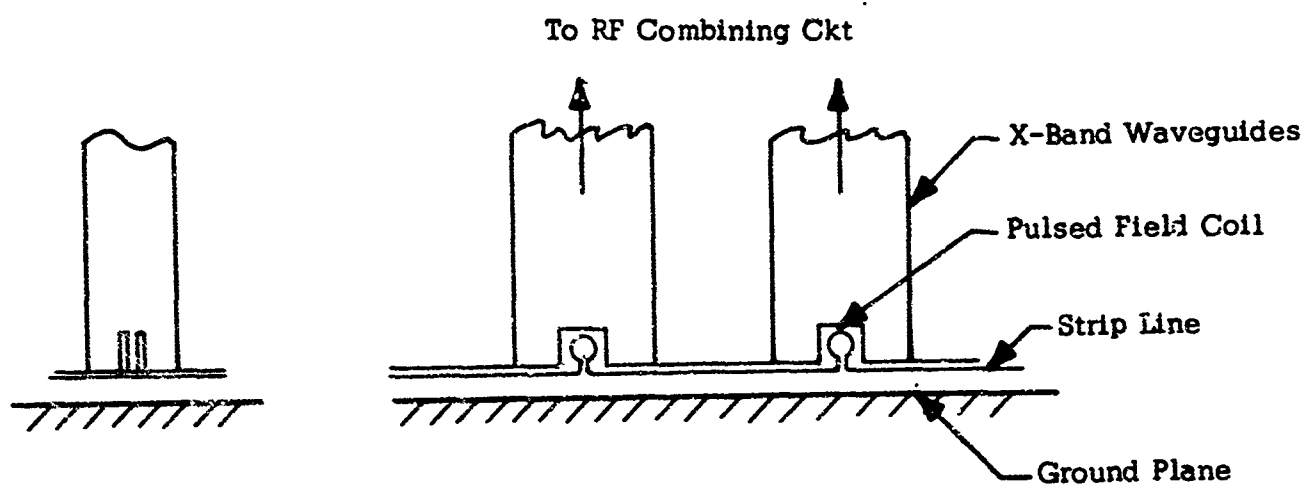


Fig. 3. Slotted pulsed-field coils in series with ungrounded conductor of pulsed-current strip line.

would take off the RF energy generated by the sphere in each loop, and an RF combining circuit would provide individual phase delays for coherently adding the individual contributions.

Instead of having the individual waveguides and the combining circuit of Fig. 3, one could have a single waveguide propagating parallel to the strip line as illustrated in Fig. 4. This guide then requires some kind of loading so the velocity of RF waves in the guide equals the velocity of propagation of the current pulse in the strip line.

The main reason for deciding against these series loop schemes is the effect of the series inductance of each loop, L , on the leading edge of the current pulse traveling down the strip line. As conceived, the leading edge of the current pulse would continuously lose steepness after passing each loop. However, it appears to be possible to add a small shunt capacitance on either side of each loop such that the effective surge impedance of the strip line appears to have no discontinuities. Unfortunately, although the steep wavefront of the total current would thus be preserved, the currents in the individual loops would not have a steep leading edge. Quantitatively, $C = L/Z_0^2$ is the total shunt capacitance to be added per loop and $f_c = Z_0/2\pi L$ is the frequency above which the capacitor current exceeds that in the loop; i.e., the capacitors "bypass" the inductors. For $Z_0 = 7$ ohms and $L = 10^{-9}$ henry, for example, the bypassed high-frequency current components are those above 10^9 Hertz. It should also be mentioned that the magnitude of the pulsed current in a loop that is in series with the line is only half that of a loop which short-circuit-terminates the line.

C. Use of Strip Line Without Loops

The next schemes considered, following a suggestion by H. J. Shaw of Stanford, are ones in which the strip line carrying the pulsed current has no discontinuities. Ferrite spheres are spaced periodically in the interior of the uniform video line embedded in a high-dielectric strength material.

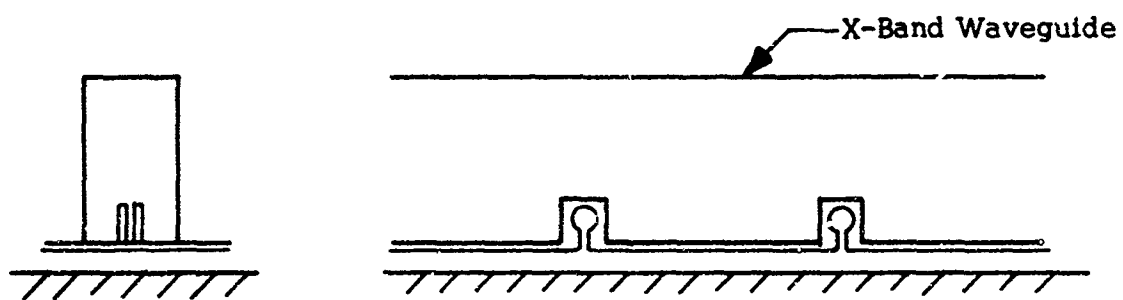


Fig. 4. Same as Fig. 3, but with a common output waveguide.

If the cross-sectional dimensions of the transmission line are the same as the cross-sectional dimensions of the pulsed-field coil used for single-sphere operation, the pulsed magnetic field seen by a ferrite sample located at the center point of the cross section of the uniform video transmission line will be nearly the same as that for the same current in the pulsed-field coil.

Since the transmission line constitutes essentially a uniform propagating structure for the pulsed-field current, the pulsed-field wave-shape will remain constant as the current pulse propagates along the transmission line, so that all ferrite samples will see substantially the same pulsed-field rate of rise, as well as other pulsed-field characteristics.

Since the pulsed-field coils have now been eliminated, with the integral slot-resonator for coupling to the ferrite, new coupling methods must be developed. In addition, methods for combining the outputs of the several spheres must be incorporated in the RF structure. Coupling, between a waveguide and one sphere embedded in a strip line, was the first measure of usefulness of a configuration. This provided a reference degree of coupling against which other configurations could be compared. The original slotted loop was attached to a rectangular waveguide short (Fig. 5, lower right). Adding a YIG sphere (0.023 inch diameter) and suitable magnetic field, the relative height of the magnetic-resonance line was observed on the scope in a reflectometer setup at X-band. When, with some other structure one observes a much weaker resonance line, that structure is less desirable. Any advantage due to a plurality of spheres is lost when the coupling to the individual spheres is weak.

The RF magnetic field generated by a YIG sphere in this strip line arrangement is mainly longitudinal. Thus the strip line does not strongly shield this field. A TE_{011} -mode circular guide resonator would therefore be expected to couple well to a sphere in a symmetrical strip line inserted along the resonator axis. The disadvantage is that these resonators would need to be long axially (over $\lambda_0/2$) and the total length of strip line would be excessive. A shorter cavity



Fig. 5. Pieces of "cold-test hardware" representing three different experiments. Top: Waveguide with tilted half-wave resonator slots in the narrow wall. Lower Left: Resonator cavity with axial H field and of short axial dimension. Lower Right: Original structure used as reference structure.

with axial magnetic fields is shown in Fig. 6. If successful, combining circuitry for the several loop outputs would still be needed. Sample cavities of this type were made (Fig. 5, lower left) and one showed a resonance near the expected frequency. However, difficulty in coupling to it suggested an inadequate loop or a very low Q_0 , or both. Inserting the YIG sphere (without strip-line conductors) did result in a coupling between its magnetic resonance and the RF resonator, but this coupling was extremely weak in comparison with coupling in other structures.

An advantage of the periodic structure of Fig. 7 (also Fig. 5, top) is the short axial length. This structure consists of diagonal (45°) half-wave slots in the thinned-down narrow wall of an X-band waveguide. At frequencies near slot resonance, electric and magnetic fields build up near the slots and provide coupling to YIG spheres located near each slot. In addition, the waveguide becomes dispersive at these frequencies and it may be predicted that for some frequency near resonance the guide phase velocity for RF would match the strip-line velocity for the current pulse.

Unfortunately, this structure had to be abandoned because the coupling to a YIG sphere placed opposite a slot was extremely weak. (To move the sphere into the slot would be to ignore the strip line's presence.)

There finally evolved the structure of Fig. 8 (also Fig. 9) which more definitely incorporates a strip line into the RF structure. A length of waveguide, with a shorting plunger at one end and a composite iris at the other, is half-wave resonant. (Although the resonance was set near 9.5 GHz when testing, this structure also has the advantage of being easily tuned to other X-band frequencies. The iris size, however, might have to be changed for bands other than 9.2 to 10.0 GHz.) The YIG sphere is located in the composite iris, and it was discovered that its magnetic resonance, as indicated by Fig. 10, is coupled more strongly than in any of the structures tested, including the reference split-loop. This result may be due to the higher Q_0 of the backing cavity and the concentration of magnetic fields near the iris.

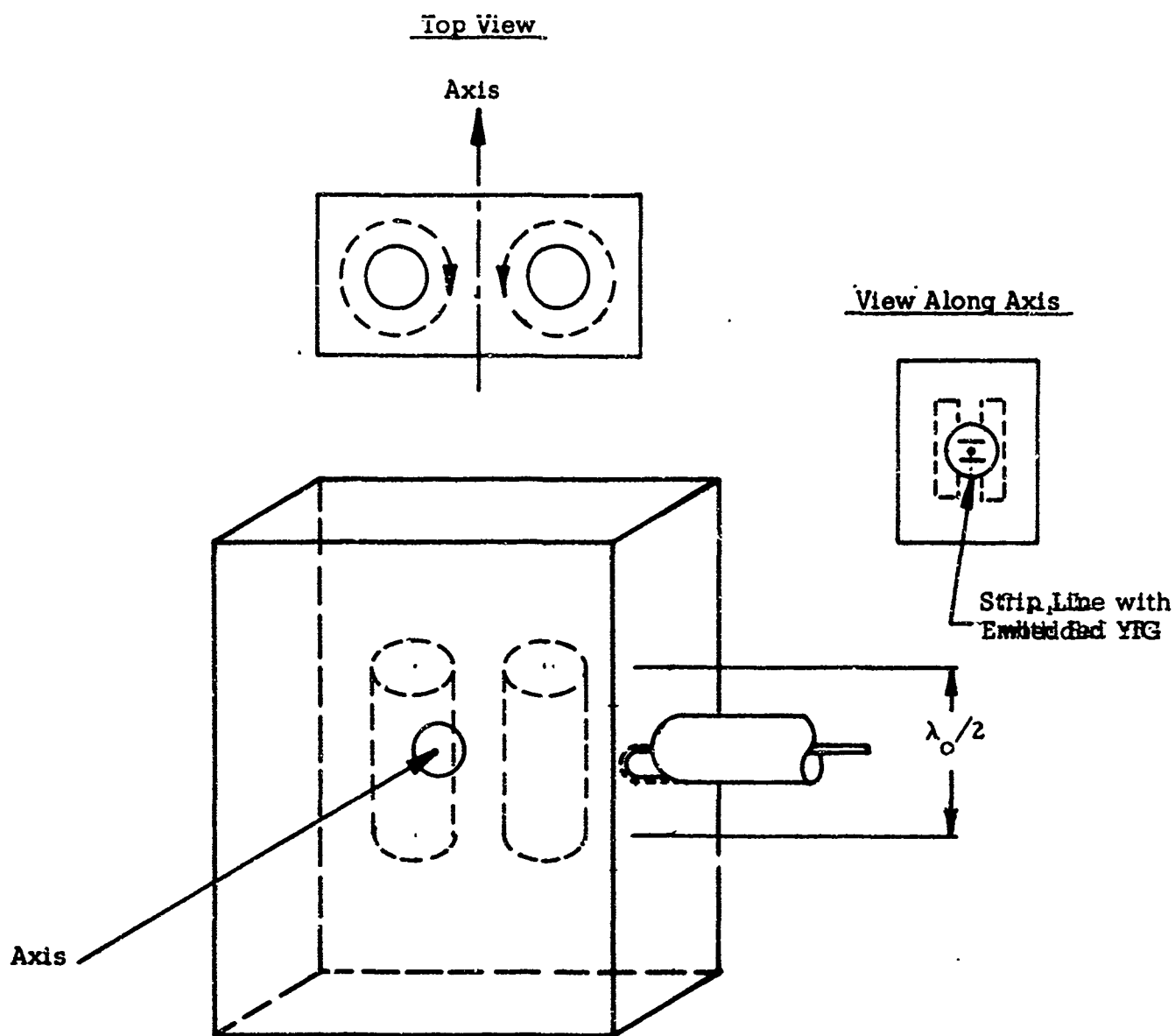


Fig. 6. Resonator cavity of short axial dimension (floating cylinders are supported by Styrofoam).

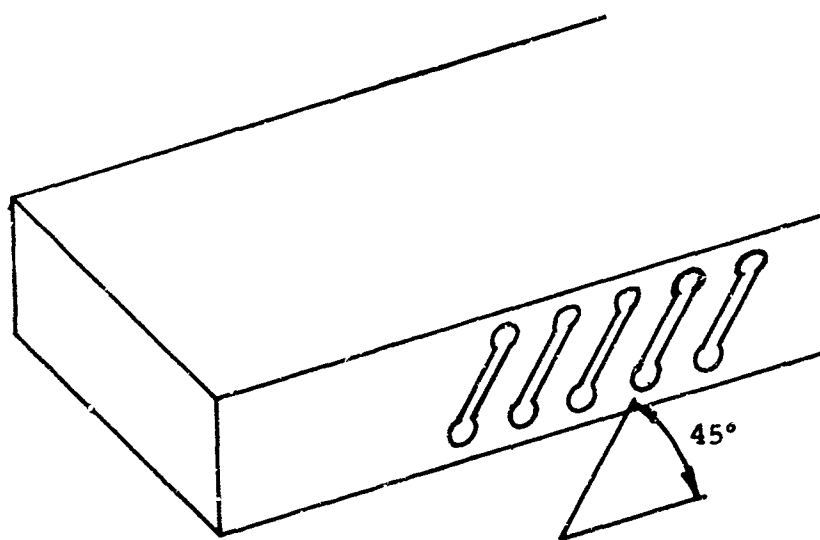
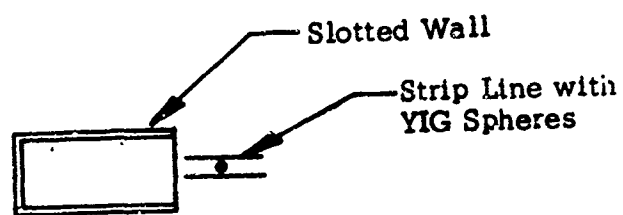


Fig. 7. Waveguide with tilted half-wave resonator slots in the narrow wall.

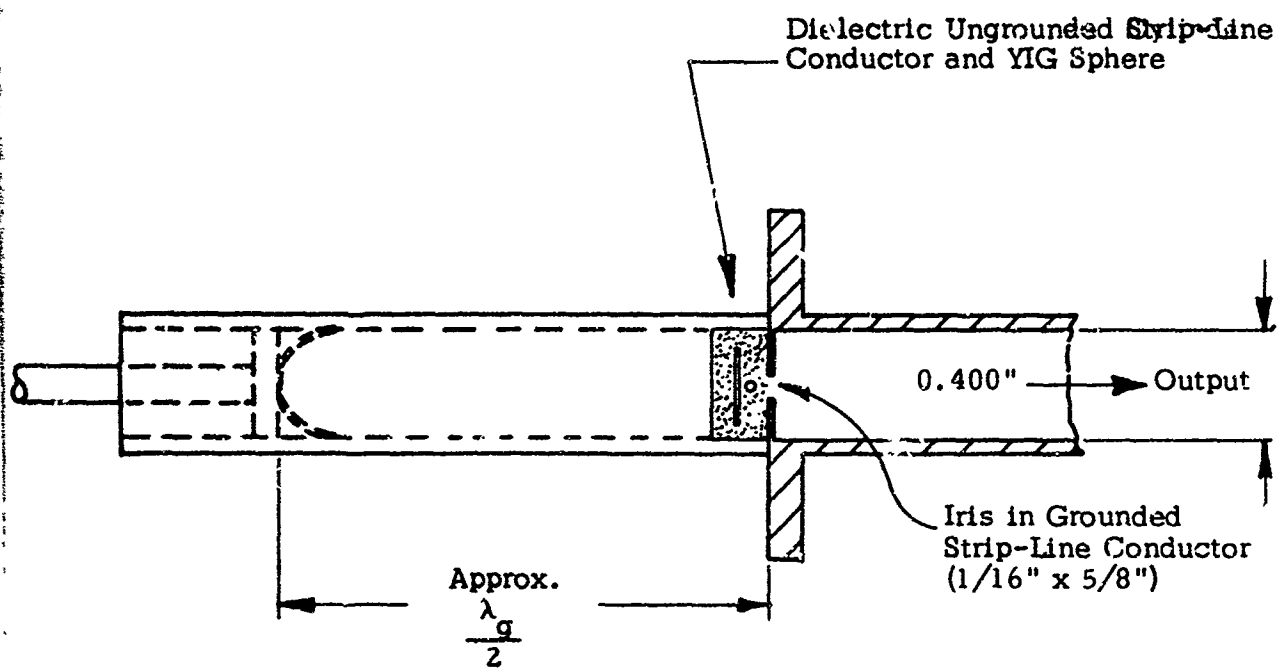


Fig. 8. Structure derived from a longitudinal slot (iris) in the ground side conductor of a strip line.

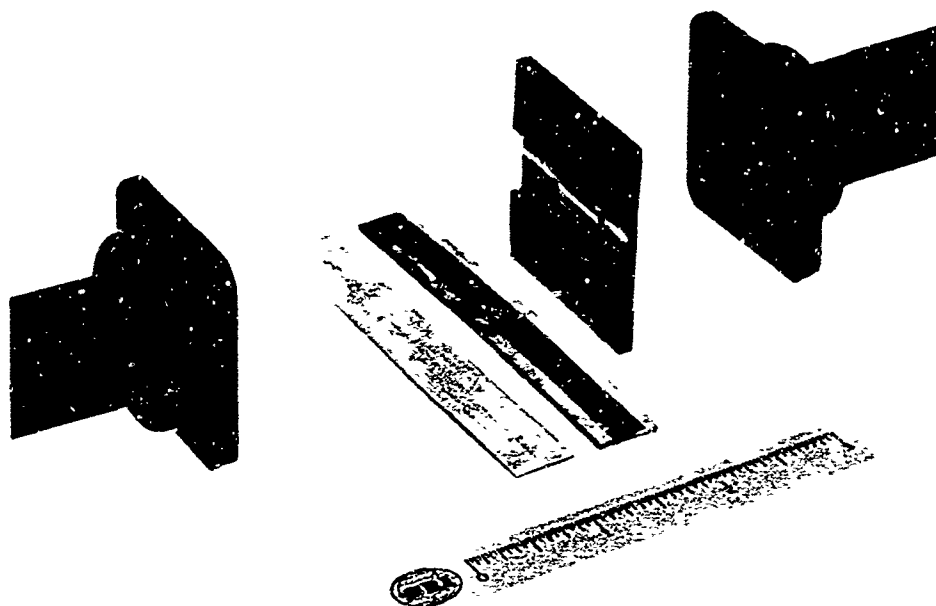


Fig. 9. Structure of Fig. 8, disassembled. Iris and metal and dielectric parts of strip line are in the center.

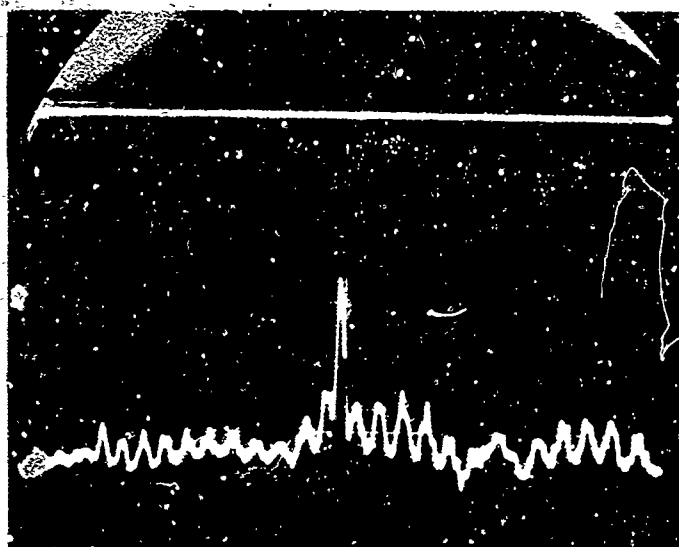
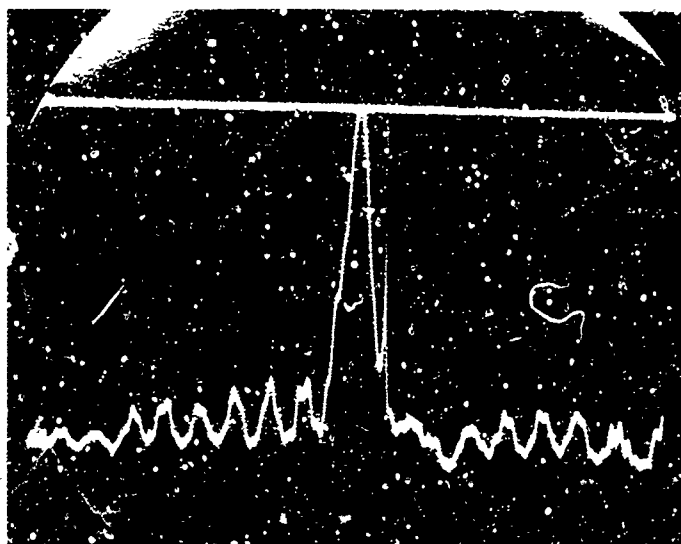


Fig. 10. Reflectometer oscillograms looking into structure of Figs. 8 and 9. Narrow absorption is ferrimagnetic resonance, broad absorption is due to back-up cavity. Ferrimagnetic resonance is approaching cavity resonance from above. Total frequency sweep is 4 GHz; center frequency is 9.5 GHz (above) or 10.8 GHz (below).

One way to utilize the new structure with multiple spheres is to use a spacing of 1 inch between spheres, irises, backing cavities, etc. If there are individual output waveguides, a combining network would be needed. If the outputs can be combined in one waveguide as shown in the photos of Fig. 11, this waveguide would require dielectric loading so that the phase velocity in the guide would equal the velocity of the current pulse on the strip line. However, the common output guide is already loaded by irises backed up by resonators, and it is difficult to establish what other loading is needed.

Another difficulty in this multi-sphere scheme is that the backing cavities take up needed room, so far as applying the dc biasing magnetic field is concerned, since this dc field must be applied at 90° to the RF magnetic field.

The final design of the RF portion of the multisphere depends upon the feasibility and final dimensions of the uniform strip line that provides the pulsed magnetic field to the YIG spheres. Work on Darlington charged-line pulsers to be used for this uniform strip line approach is described in the next section.

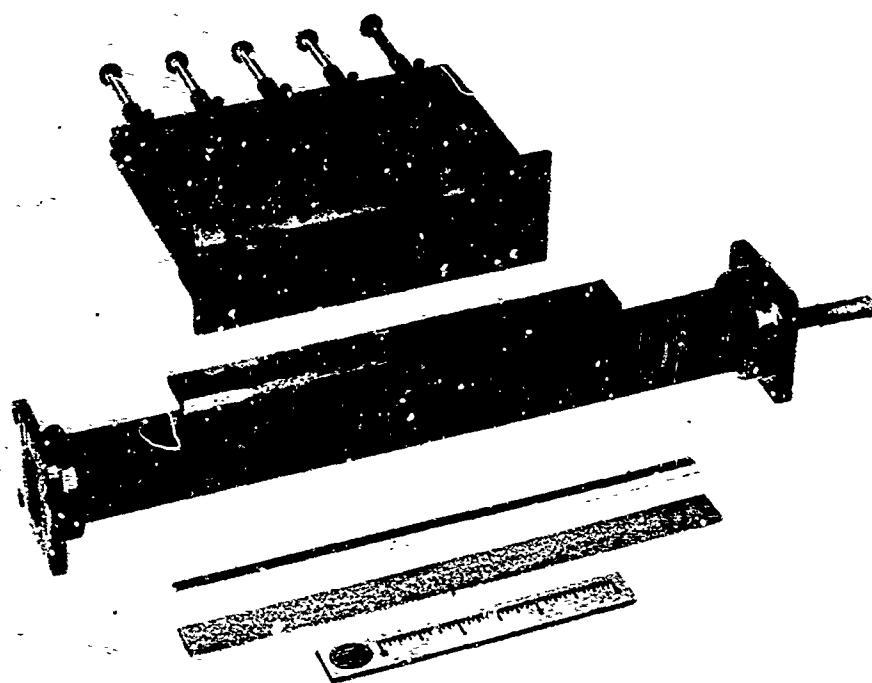


Fig. 11. "Cold-test hardware" with strip line, irises and back-up cavities. Development of structure of Figs. 8 and 9 with five irises feeding common output waveguide.

III. DARLINGTON PULSER

The multiple-sphere generator technique employing a uniform line to generate the pulsed-magnetic field as described in Part II, imposes severe requirements on the pulser. These arise since (1) the pulser output line is now terminated so that current doubling does not occur as in the single-sphere case where the coil effectively shorts the line, and (2) the characteristic impedance Z_0 of the video line is now approximately a factor of ten larger than for the single-sphere case. Z_0 is high since the uniform line must be the same width as the pulsed-field coil to obtain the same magnetic field-to-current ratio, $H/I = 2.75 \text{ Oe/A}$, as the coil.

For a strip-line width equal to the coil width of 112 mils, and a strip-line spacing equal to the YIG sphere diameter of 48 mils, Z_0 is 90 ohms for a dielectric constant of about 3. Assuming that the YIG sphere can be partially placed in indentations in the strip line, a strip-line spacing of 24 mils and an impedance on the order of 45 ohms will be obtained. For operation up to 10 GHz, a pulse current of 1300 amperes is required for terminated video line operation. The pulse voltage required to supply this current in a 45-ohm line is then on the order of 60 kV.

The strip-line dielectric must therefore withstand E-fields of 2.5 kV/mil. High dielectric strength materials have been investigated. Although it appears that Mylar immersed in Freon C-138 may be satisfactory (see DuPont Bulletin M-4C) the effects of nonlinearities on pulse shape must be evaluated. Other methods such as quartz-clad molybdenum may also be feasible. The fact that pulse widths are only 2 ns is expected to help the breakdown problem since the breakdown mechanism has insufficient time to cause sparking².

Due to the high pulse voltage requirements for the multiple-sphere technique described above, multiple-line types of charged-line pulsers in which the pulse output voltage can be larger than the dc charging voltage were investigated. Two experimental models of the Darlington pulser^{3,4}, which uses a stepped impedance pulse-forming line, were constructed and tested. The ratio of pulsed to dc voltages is theoretically $N/2$, where N is the number of steps.

The first model was a strip line constructed with six steps of 2.5, 7.5, 15, 25, 37.5, and 2.5 ohms for a load impedance of 45 ohms. This load impedance is the required Z_0 of the uniform line of the multiple-sphere circuit.

The lengths of the line between steps was 6.25 inch, which theoretically should result in a 2 ns pulse width. The measured pulse width at 50 percent pulse amplitude was 8 ns with a rise time of 2.5 ns. The ratio of pulse to dc charging voltage, V_p/V_0 , was 0.75 rather than the expected value of $N/2=3$.

The second Darlington pulser built had line lengths of 12.5 inches between steps. This increased line length was tried because it was suspected that the low pulse voltages were due to the slowness of the closing of the spark-gap switch relative to the pulse width; i.e., the switch was not completely closed before the first reflection from the first stepped-impedance junction arrived at the switch. The measured ratio of pulsed to dc voltage for the second pulser was 1.0. If there were no line losses, and if optimum line impedances were used, a ratio of 1.75 could be expected. Since this is 60 percent of the theoretical value expected for a perfect switch, the rest of the pulse reduction can be attributed to losses in the switch resistance. The spark-gap resistance is a decreasing function of time due to gas ionization time. A switch resistance of 1.8 ohms, at times comparable to pulse lengths of 4 ns, can account for the 40 percent reduction in pulse voltage.

Assuming that a 60 kV pulse voltage is wanted, a dc charging voltage V_0 on the order of 60 kV is required for $V_p/V_0 = 1.0$. This is a reasonable improvement over the normal charged-line pulsers with spark-gap switches, which have measured V_p/V_0 values of 0.35 as compared with the theoretical value of 0.5, and which would then require a dc charging voltage of 170 kV.

An exponentially tapered line pulser with a separate 12.5-inch pulse-forming line was also constructed. The impedance taper was the same as the stepped Darlington line. Pulse-to-dc voltage ratios were much the same as for the Darlington pulser.

IV. FEASIBILITY OF SOLID-STATE SWITCHES

A. Introduction

A high-amplitude pulsed magnetic field with a steeply rising leading edge is necessary if significant output powers and reasonable efficiencies from pulsed ferrite microwave sources are to be realized. The present approach is to use a system of transmission lines and spark gaps to generate a steeply rising current pulse. Because of the difficulties in obtaining stable operation from a charged-line pulser with spark-gap switches, and because of the gradual degradation of the gaps due to erosion, other techniques for obtaining a fast, large-current switch have been considered.

The switch for the pulsed ferrite microwave system must be capable of switching large currents in very short times. Realization of the specific switch specifications (Section B-1) with a solid-state device would represent a significant advance in the present state of the art. The aim of this study is to determine the feasibility of using known solid-state phenomena to accomplish the desired switching function.

B. Technical Considerations

In the following sections, the pertinent technical aspects of the dynamic switching characteristics of the PIN diode, the "glass" switch, and the thyristor, are considered with respect to the requirements of the pulsed ferrite microwave system. Each of the devices considered is substantially homogeneous in the plane perpendicular to the flow of current. Therefore, the current-carrying capacity can be increased by increasing the lateral area of the device. In this survey, only the switching speed and the voltage-blocking capability of the respective devices has been considered as crucial to the application. In general, ultimate switching speeds have not been achieved in practice for these devices. The purpose here, then, is to make a best estimate of ultimate switching speeds using existing theoretical models.

1. Switch Specifications

The specification for the switch are derived from the present concept of the system, using spark gaps. Because the primary requirement for a steeply rising current pulse dictates the over-all system design to a large extent, any candidate for a switch will have to operate under similar conditions.

The switch specifications are most conveniently described in terms of the required current pulse as depicted in Fig. 12. The leading edge is the most important part of the pulse with respect to the operation of the ferrite microwave generator and must satisfy the following conditions:

$$\tau_1 < 1 \text{ nsec}$$

$$\tau_2 < 1.5 \text{ nsec}$$

$$I_t > 1500 \text{ amperes}$$

200 pps repetition rate minimum

The over-all pulse duration is important only in determining the dissipation of the switch and the minimum repetition rate.

Because circuit inductance is expected to be of the order of one nanohenry, switch resistance should be of the order of 10 ohms or less to limit dissipation in the switch and to minimize the voltage required to obtain the necessary current level.

2. Thyristors

Thyristor is a generic term referring to a family of multilayer semiconductor switching devices. Thyristors include such classes of solid-state switches known as four-layer diodes, semiconductor controlled rectifiers (SCR's), and the triac. They are often referred to as p-n-p-n switches. The latter name is appropriate because it serves to describe the major constructional feature that is common to all thyristor devices.

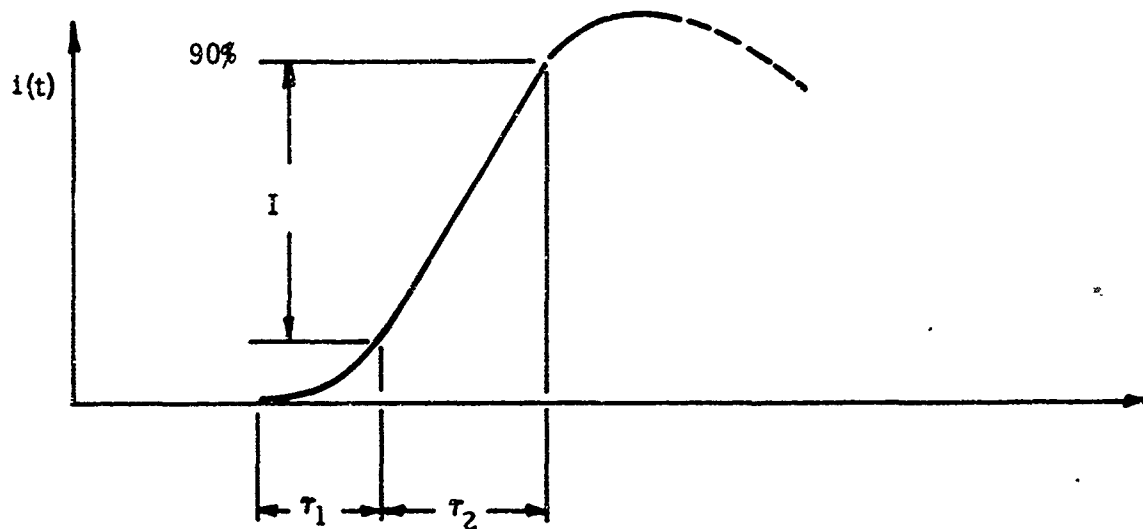


Fig. 12. Leading edge of typical current pulse required by the pulsed ferrite microwave system.

At the present time, thyristor devices (mainly SCRs) are available with current ratings up to 1000 amperes. Blocking voltage ratings extend to above 1000 volts and power-handling capabilities of over 200 kW can be obtained. It appears that the current and voltage specifications of presently available thyristor devices nearly satisfy the system requirements for the pulsed ferrite microwave source. However, most thyristor devices in use today are in the SCR class and as such are seriously limited in switching speed--as discussed in subsequent paragraphs in this section.

The present limitations on the switching speed of SCRs are related to the triggering method and to the physical construction of the devices; it is not an intrinsic limit applicable to all thyristor devices. Therefore, major emphasis in this portion of this study has been put on estimating the ultimate switching speeds to be expected for thyristor devices. Because the ultimate switching speed depends on the technique used to trigger the thyristor into the low-impedance state, each trigger technique will be considered separately.

There are four methods whereby thyristors may be triggered from the high-impedance state into the low-impedance state. These are:

- gate triggering,
- dv/dt triggering,
- avalanche breakdown of the center junction or simply voltage triggering, and
- triggering by punchthrough.

Estimates of the ultimate switching speed for each of the triggering modes can be made by using the one-dimensional model and analysis introduced by Moll, et al⁵ and elaborated by Gentry, et al⁶. To point out the important mechanism on which the switching speed depends, a brief summary of only the necessary aspects of the theory follows.

Figure 13 shows the thyristor structure schematically and the two-transistor analog normally used to explain the basic switching action. When the thyristor is in the high-impedance state, junctions J_1 and J_3 are forward biased. Junction J_2 is reversed biased so that most of the terminal voltage appears across it. The two-transistor analog in Fig. 13 indicates the presence of a positive feedback loop. If the current transfer ratios, α_1 and α_2 are large enough, then an increase in the emitter current of either transistor causes an increase in the base current of the other and subsequent regeneration of the increase in the first transistor. Analysis of the two-transistor analog shows that the regeneration effect occurs when $\alpha_1 + \alpha_2 = 1$. Because the current transfer ratio depends on the magnitude of the emitter current, the thyristor can be triggered from the high-impedance state to the low-impedance state by any mechanism which causes sufficient current to flow through either J_1 or J_3 such that the condition $\alpha_1 \alpha_2 = 1$ occurs. For example, current flowing into Gate 2 and out of the cathode also flows across J_3 and may cause the thyristor to switch. A similar condition can occur if current flows into the anode, through J_1 and out of Gate 1. These are examples of gate triggering and are explained in more detail in the next section.

a. Gate Triggering

Because most thyristor applications now involve gate triggering, the theoretical and practical aspects of this triggering mode are understood best. With gate triggering, the switching speed can be affected in two distinct ways. One limitation on the switching speed is the time required for a small initial "turned-on" region to spread laterally across all of the intended active area of the device. A second, more fundamental limitation, is the time required to redistribute the charge in the various layers of the device.

(1) Lateral Spread of Active Region

In present thyristors (SCRs), designed to switch large currents, the "turned-on" region spreads laterally away from the point where the gate connection is made; this is illustrated schematically in Fig. 14. The primary cause of the lateral

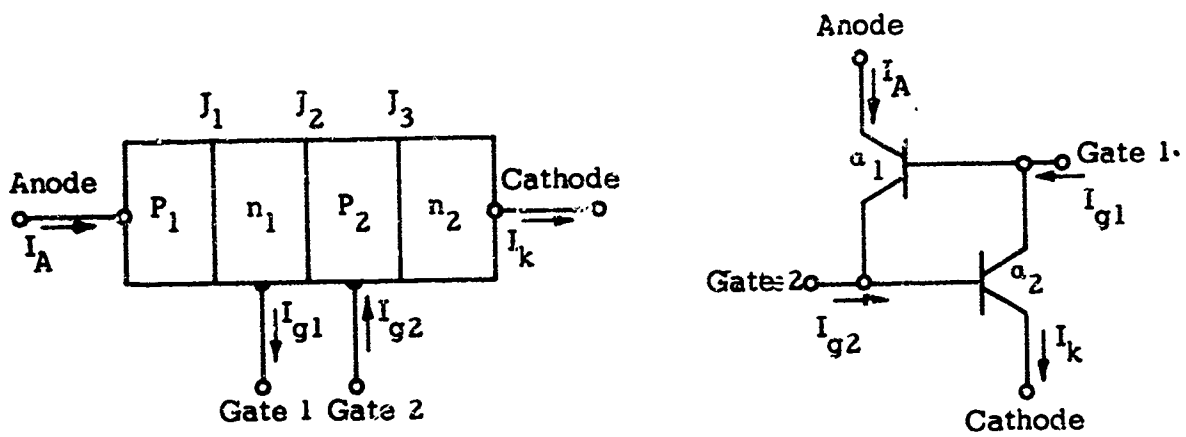


Fig. 13. Schematic of the thyristor and the equivalent two-transistor analog.

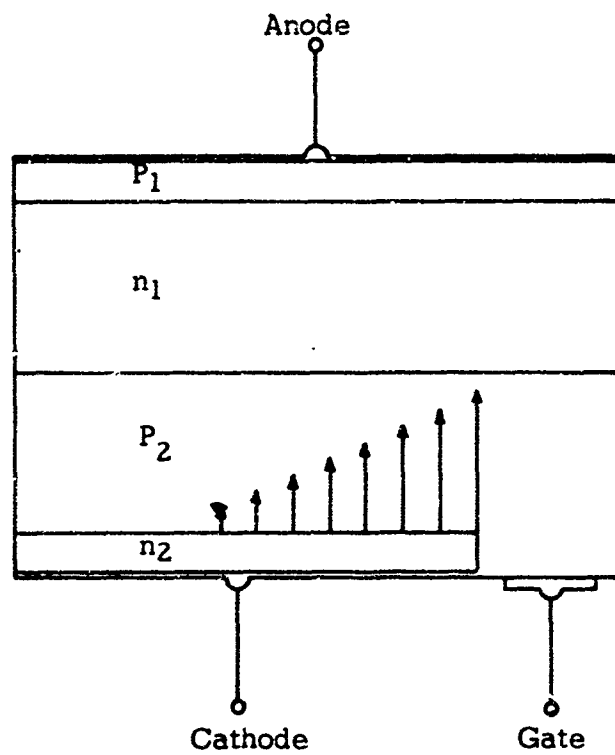


Fig. 14. Illustration of the lateral spread of the "turned on" region in an SCR.

spread is the transverse resistance of the base, p_2 . In situations where the gate connection is attached to one point off to the side, the closest part of the cathode (n_2) will conduct the largest portion of the gate current. Consequently, the conditions for initiating the regeneration effect that leads to switching will occur first in the region closest to the gate connection and then spread by diffusion over the rest of the device. Reduction in the turn-on time due to lateral spread can be obtained by improving device geometry through the use of multiple base connections or an interdigitated structure such as described by Davies and Petruzella⁷.

Localized turn-on and the accompanying slow switching can also be caused by lateral inhomogeneities in the semiconductor material from which the thyristor is made. If the inhomogeneities are severe enough, the "turn-on" region may not propagate over the entire area of the device.

Because the lateral spread of the active region depends only on the geometry and homogeneity of the material from which the thyristor is made, it is not an intrinsic limit on the switching speed. Therefore, no attempt has been made to estimate switching speeds due to lateral spread. It can be expected that future improvements in device fabrication techniques will eliminate the present importance of lateral spread for the case of gate triggering. In addition, there is strong evidence that local turn-on and lateral spread do not occur when other triggering methods are used (provided that the material is relatively homogeneous in the plane transverse to current flow).

(2) Charge Redistribution

Analysis of a one-dimensional, gate-triggered thyristor has been recently made by Davies and Petruzella⁷. They described the dynamic conditions during switching in terms of changes in the charge distribution in the four layers of the device. The portion of their analysis that pertains to application of the thyristor as a switch for the pulsed ferrite microwave generator is summarized as follows.

During switching from the high-impedance state to the low-impedance state, the current increase can be characterized by two regions--a delay time and a current rise as depicted in Fig. 15. The delay time is identified as the time required to reach a charge distribution such that the center junction (J_2) is just reaching a condition of zero bias and the current increase is nearing the maximum rate. It appears that, for most thyristors, the current level at the end of the delay time (point "a" in Fig. 15) will be less than 10 percent of the final value. For this condition, the rise time of the current will be nearly that occurring during the rapidly changing portion of the characteristic.

The analysis of Davies and Petruzella indicates that only circuit inductance limits the maximum attainable rate of current rise in circuits using thyristors. The $L(di/dt)$ product is then the supply voltage minus the high-field voltage drop across the thyristor. Apparently, the thyristor can be designed so that the high-field voltage drop is only a small percentage of the blocking voltage. Therefore, the $L(di/dt)$ product can be increased by designing thyristors with increased blocking voltage capabilities.

(3) Summary

Commercial thyristors, with current and blocking voltage ratings nearly adequate for the pulsed ferrite microwave generator system, are presently available. The switching speeds are slow, however, because of the delay associated with the lateral spread of the active region. The analysis of Davies and Petruzella indicates that the intrinsic limit on the switching speed depends upon the circuit more than upon the thyristor. Therefore, improved geometry and device quality should make high-speed thyristor switches possible.

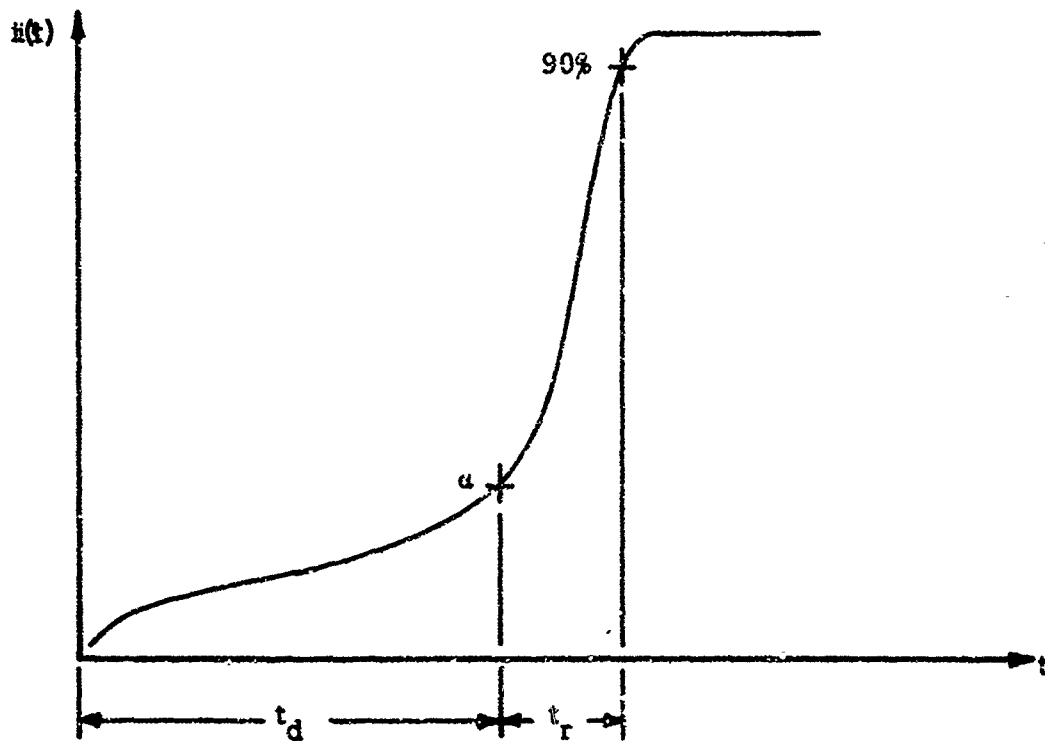


Fig. 15. Typical current increase during gate-triggering for an ideal SCR.

b. dv/dt Triggering

Thyristors may be triggered from the high-impedance state to the low-impedance state by the application of a rapidly rising voltage at the device terminals. (A gate connection is not used for this triggering mode.) When the device is in the high-impedance state, J_1 and J_3 are forward biased and J_2 is reverse biased (Fig. 13). A rapidly rising voltage pulse at the thyristor terminals will cause a displacement current to flow through the capacitance of J_2 and consequently through the junctions J_1 and J_3 . If the magnitude of the current through J_1 and J_3 is sufficient to cause the sum of the alphas to increase to unity, the thyristor will switch to the low-impedance state. Once this point has been reached, the switching dynamics are substantially the same as during the current rise portion of the switching cycle under gate triggering. The current during the delay and the delay time (Fig. 15) depend primarily on the rate of voltage rise.

Two disadvantages occur because of triggering by dv/dt : (1) transients in the system can cause false triggering, and (2) the triggering current must flow through the load. Typically, the thyristor would be biased to a large percentage of its blocking voltage and a fast triggering pulse would be superimposed to promote switching. For application in the pulsed ferrite system, the thyristor must have a large current amplification ratio when triggered by dv/dt . Because the triggering current flows through the load circuit, the trigger current level should not exceed 10 percent of the final load current if the rise time is to depend only on circuit parameters as in the gate-triggered case.

The greatest advantage of using dv/dt triggering with present thyristors is the elimination of problems due to lateral spread of the active region. Experimental results⁸ have shown that if the rate of voltage rise is great enough, the thyristor will turn on uniformly and full advantage of the total device area is obtained for current-carrying capacity.

c. Avalanche Breakdown

The thyristor can be triggered to the low-impedance state by avalanche breakdown, which represents a potentially useful means for obtaining large di/dt values during switching. The center junction of the thyristor is reverse biased when in the high-impedance state and, by slowly increasing the total voltage across the thyristor terminals, the center junction can be brought to the condition where avalanche breakdown occurs (provided the device is designed to avalanche before punch-through occurs). Under these conditions, the thyristor and the p-i-n diode (discussed in V-C) can be analyzed by the same techniques, and estimates of the di/dt rates can be made for both, using the simplified model as follows.

The process that initiates the avalanche breakdown is shown schematically in Fig. 16. An electron that diffuses from the p-region and enters the space-charge region is accelerated by the electric field until it reaches an energy sufficient to cause a secondary emission of an electron when a collision with the crystal lattice occurs.* The initial and the secondary electrons are then accelerated by the electric field and the process repeats, creating a growing number of electrons until the current is limited by the external circuit.

The rate of rise of current in the external circuit can be estimated from ionization rates for silicon which are expressed in terms of α , the ionization probability per centimeter per electron. (For example, see J.L. Moll, "Physics of Semiconductors", McGraw-Hill, 1964, p. 222.)

*Holes and electrons both take part in the avalanche process. When an ionizing collision takes place, hole-electron pairs are created. In silicon, the ionization rates for electrons is roughly an order of magnitude greater than for holes; therefore, the rate of current increase depends primarily on the electron processes.

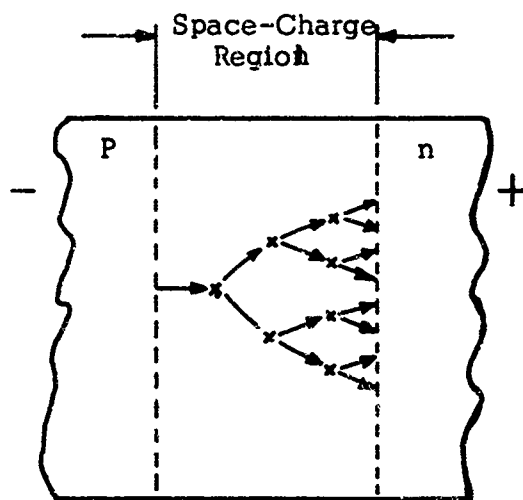


Fig. 16. Schematic representation of the avalanche multiplication process in a reverse biased p-n junction.

The time between collisions is given by

$$\tau = \frac{1}{\alpha \langle v \rangle} \quad (1)$$

where $\langle v \rangle$ is the average velocity of the electron. The current density is proportional to the density of carriers crossing the depletion region and the carrier velocity, viz

$$i = qn \langle v \rangle \quad (2)$$

where q is the electronic charge and n is the number of electrons/cc in flight. During the onset of avalanche, n doubles each time a collision occurs; therefore, the time dependence of n may be expressed as

$$n(t) = n(0) 2^{t/\tau} \quad (3)$$

where $n(0)$ is the density of electrons entering into the avalanche process at $t=0$. Equations (1) and (3) combine to yield

$$i(t) = qn(0) \langle v \rangle 2^{t/\tau} \quad (4)$$

If i_2 and t_2 represent the current and time respectively for the condition when the current is 90 percent of the final value, and i_1 and t_1 represent the current and time respectively for the condition when the current is 10 percent of the final value.

$$\frac{i_2}{i_1} = 9 = 2^{(t_2 - t_1)/\tau} \quad (5)$$

The rise time is then

$$t_2 - t_1 = \tau (\log 9) / (\log 2) = 3.2\tau \quad (6)$$

It is assumed that the incident and secondary electrons are at zero drift velocity immediately after an ionizing collision; i.e., the collision absorbs all of the field-derived energy of the incident electron. It is also assumed that no non-ionizing collisions occur between ionizing collisions. The average drift velocity, then, is one-half the velocity of the electron just before it suffers an ionizing collision. Published data relating α and the electric field in the depletion

region indicate that the field strengths required for avalanche breakdown insure that the electron is traveling at or near the saturated drift velocity for the material. For silicon, the saturated drift velocity is about 10^7 cm/sec and α varies from $2 \cdot 10^2$ to $2 \cdot 10^5$ cm⁻¹ so that τ varies from $5 \cdot 10^{-10}$ to $5 \cdot 10^{-12}$ seconds.

Rise time due to avalanche breakdown in silicon p-n junctions can be expected to range from 1 to 2 nanoseconds to as low as 3 picoseconds.

d. Punch-through

The external characteristic of the thyristor triggered by punch-through is similar to that obtained with avalanche breakdown. If the terminal voltage is increased slowly, either punch-through or avalanche breakdown will occur, depending on the width of the n_1 region in Fig. 13. (The n_1 region is usually the higher resistivity region.) As the terminal voltage across the thyristor is increased, the reverse voltage across the center junction increases, causing the space-charge layer to widen. If the space-charge layer widens to the extent that it crosses the emitter junction, I_1 , punch-through occurs and the thyristor then switches to the low-impedance state.

No quantitative estimate of the switching speed due to punch-through has been made although it is generally thought to be on the order of that obtained for avalanche breakdown.

3. p-i-n Diode

The p-i-n diode is not suitable for a fast, high-current switch for the pulsed ferrite microwave generator system. The primary deficiency lies in the shape of the I-V characteristic (Fig. 17). A suitable switch should have an "S" shaped I-V characteristic, double-valued in current; i.e., a negative resistance region so that the switch will "latch" once triggered on. The p-i-n diode operating in the avalanche mode will have a constant voltage drop in order to sustain the

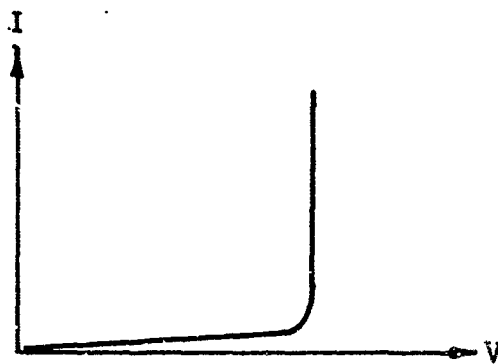


Fig. 17. Reverse voltage characteristic for a typical p-i-n diode.

avalanche mechanism. Therefore, a low impedance cannot be sustained below the trigger voltage. To apply such a characteristic requires a perfect voltage source with zero internal resistance. Clearly, any practical application is not possible.

4. Glass Switch

In September 1966, Energy Conversion Devices Company announced a switching device made from a homogeneous layer of specially prepared glass. This device (the glass switch) was reported to have switching speeds ranging from several microseconds to less than one nanosecond^{9,10}. Current-handling capabilities were reported to depend only on the device area¹⁰. Since that time, however, very little has been presented on the theoretical operation of the glass switch and almost no test data on working models have been published. Apparently, the physical basis of operation of the switch is not well understood at this time. Because of this, and in the absence of actual test data, very little can be said about the potential applications of the glass switch.

Some laboratory development of the glass switch is in process at the present time¹¹, but it appears that additional development will be required before the glass switch can be considered a usable component suitable for application by system designers. At the present stage of development, the glass switch does not appear to be a suitable candidate for switching service associated with pulsed ferrite microwave sources.

C. Summary and Conclusions

The three solid-state devices that have been considered for possible application as fast, large-current switches are:

- p-i-n diode
- "glass" switch
- thyristor (p-n-p-n switch).

The p-i-n diode operating in the avalanche mode is ruled out because its I-V characteristic does not have a negative resistance region. Therefore, it will not "latch" in the low-impedance condition when used with practical voltage sources having non-zero internal impedances.

The "glass" switch has been reported to be potentially very fast but it is ruled out for application in the near future because too little is known about the physical basis of its operation and only a small number of low-current laboratory devices have been reported on.

Of the three candidates, only the thyristor appears to have promise for application in the pulsed ferrite microwave system. The thyristor is presently in a state of rapid development for power control applications. Although commercial thyristors (SCRs) that nearly fulfill the voltage and current requirements of the pulsed ferrite microwave system are available, these devices, as presently used, lack the necessary switching speed. The slow switching speeds appear to be related to the triggering method and the physical structure of present thyristor devices and is not due to intrinsic limitations. Consideration of the fundamental aspects of the switching process indicates that switching speeds adequate for the pulsed ferrite microwave system are possible with thyristor devices.

The p-i-n diode should not be considered further. The "glass" switch should not be considered unless future developments indicate a significant advantage for rapid switching of large currents.

The potential of thyristors as fast, high-current switches should be investigated further. The results of this study indicate that the required fast switching speeds and large current-handling capabilities can be realized through proper device design and application. Furthermore, such a high-speed, large-current switch would be useful in other high-power pulse circuits and in applications such as high-power converters. The next step in the development of fast, high-power thyristor switches should be an experimental program to determine the ultimate switching speeds of present thyristor devices.

Much of the experimental and theoretical work done on thyristors to date has been concerned with the limitations attributed to the spreading of the active region when gate triggering is used. Apparently, the region of maximum current rise has not received a great deal of attention and little information regarding the ultimate switching rates of practical devices is available. It is possible, however, to eliminate effects due to active region spreading, and to determine ultimate switching speeds for presently available devices, by using dv/dt triggering or by forcing the device into the avalanche or punch-through condition.

An experimental program should be considered in which selected thyristors are tested to determine what ultimate switching speeds are presently available. Both large- and small-area devices should be included in this program to substantiate the independence of ultimate switching speed on device area. In addition, the design parameters that affect the switching speed should, where possible, be identified experimentally and compared with the present theoretical model. Based on these results, a thyristor switch for the pulsed ferrite microwave system should be designed.

V. X-BAND PULSED-FERRITE GENERATOR

A. Generator Construction

The delivered pulsed-ferrite generator was housed in a cabinet 16 inches high, 21 inches wide and 24-1/2 inches deep as shown in Figs. 18, 19 and 20. This cabinet houses two separately enclosed chassis, each with a standard 7 x 19-inch front panel. These two chassis contain the pulsed-ferrite X-band generator with its associated high current pulser and the triggering circuitry for the high current pulser. These two chassis have top and bottom covers held in place with quarter-turn fasteners for rapid access to components.

1. X-Band Generator Chassis

The X-band generator chassis contains the ferrite-pulsed-field-coil RF assembly and the 2 ns wide, 1 ns rise time, 1500A charged-line pulser required to drive the pulsed-field coil.

a. RF Assembly

The RF assembly is similar to the prototype developed by Stanford¹⁹ but has been modified thusly:

- The size of the X-band waveguide flange has been reduced to accomodate a 660-gauss horseshoe permanent magnet having a 1.1 inch gap.
- The length of the resonant slot in the pulsed-field coil, of the type shown in Fig. 1, has been increased by 75 mils so that Stycast dielectric loading in the slot is not required.
- The tuning mechanism has been changed.

A photo of the RF assembly and magnet is shown in Fig. 21. External tuning of the X-band output frequency is provided by dielectric tuning of the resonant slot

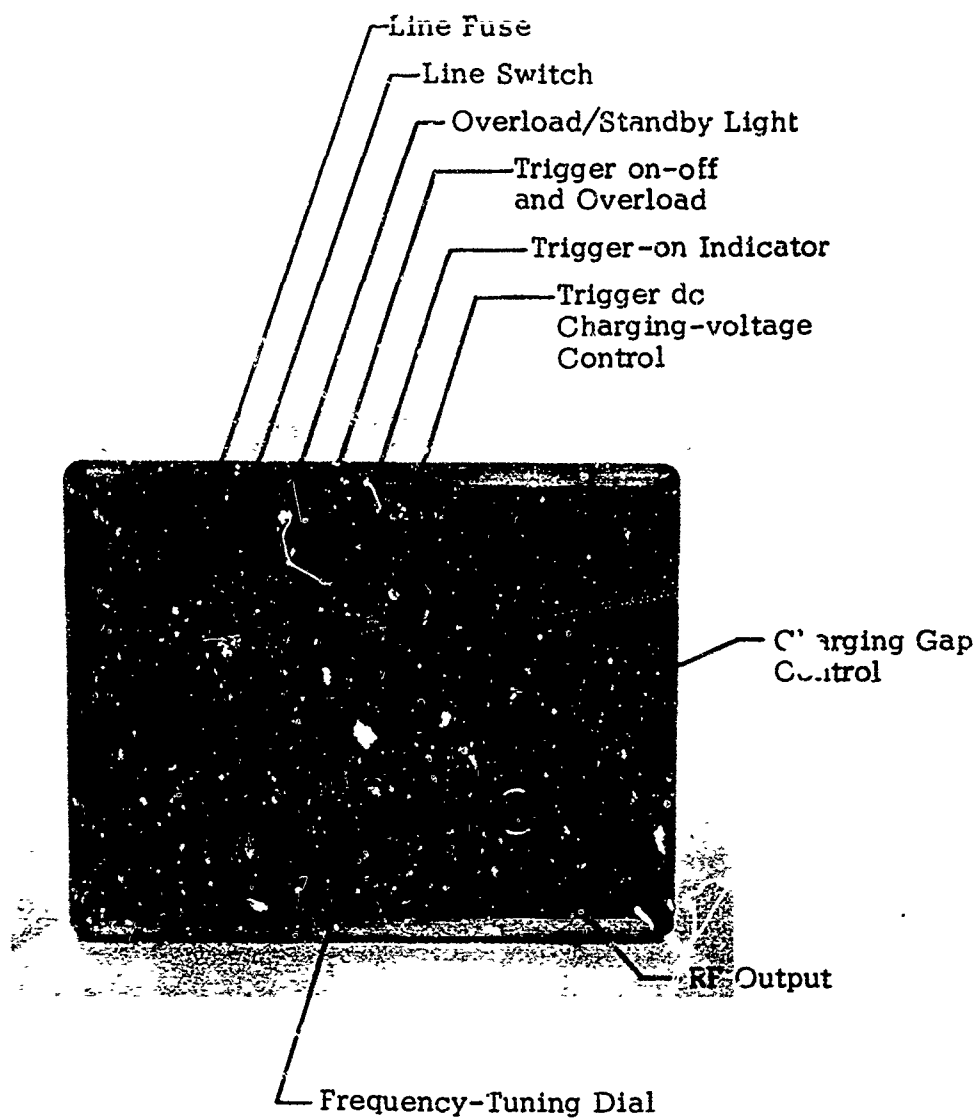


Fig. 18. Front view of the RF generator cabinet housing the pulsed ferrite X-band generator chassis (bottom) and the spark gap triggering circuit chassis (top).

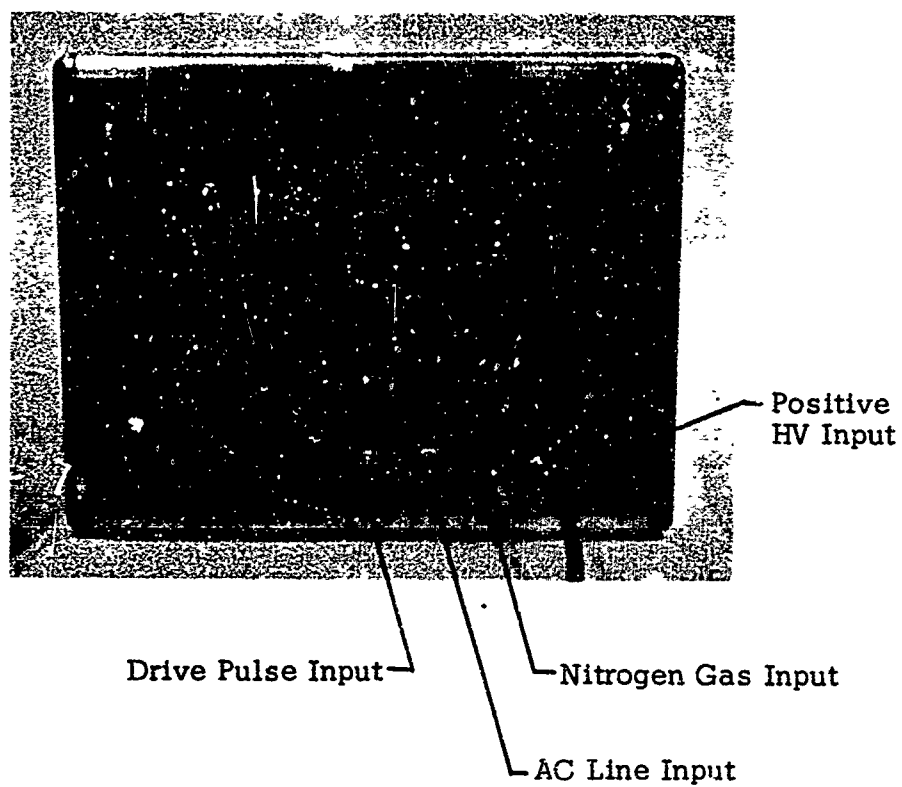


Fig. 19. Back view of the RF generator cabinet.

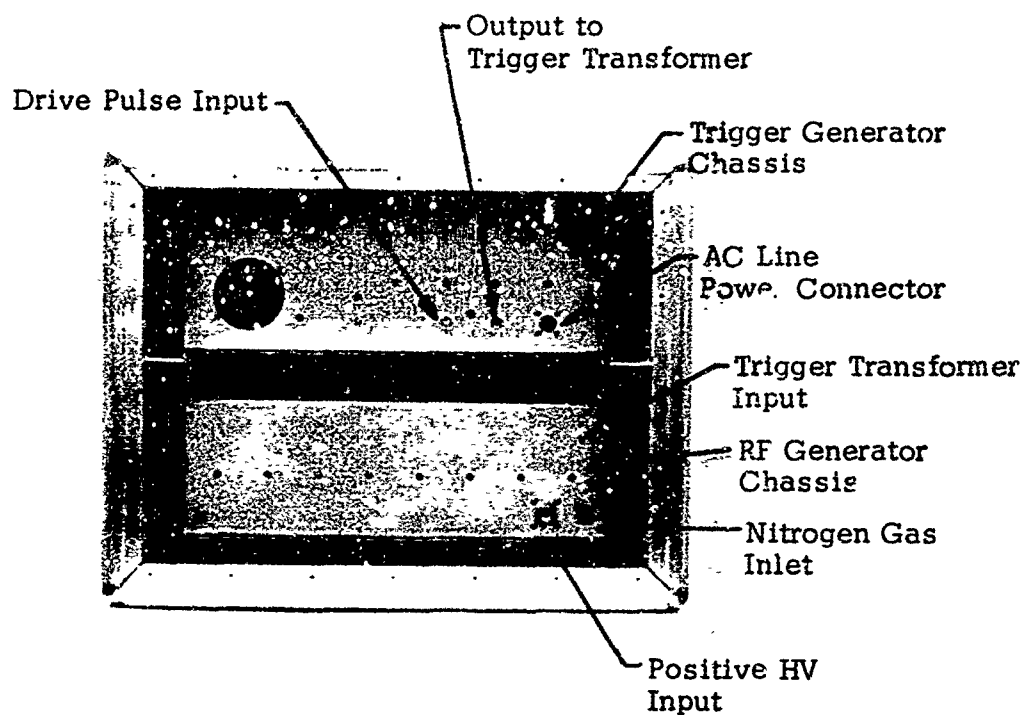


Fig. 20. Back view of the RF generator cabinet with the back cover removed.

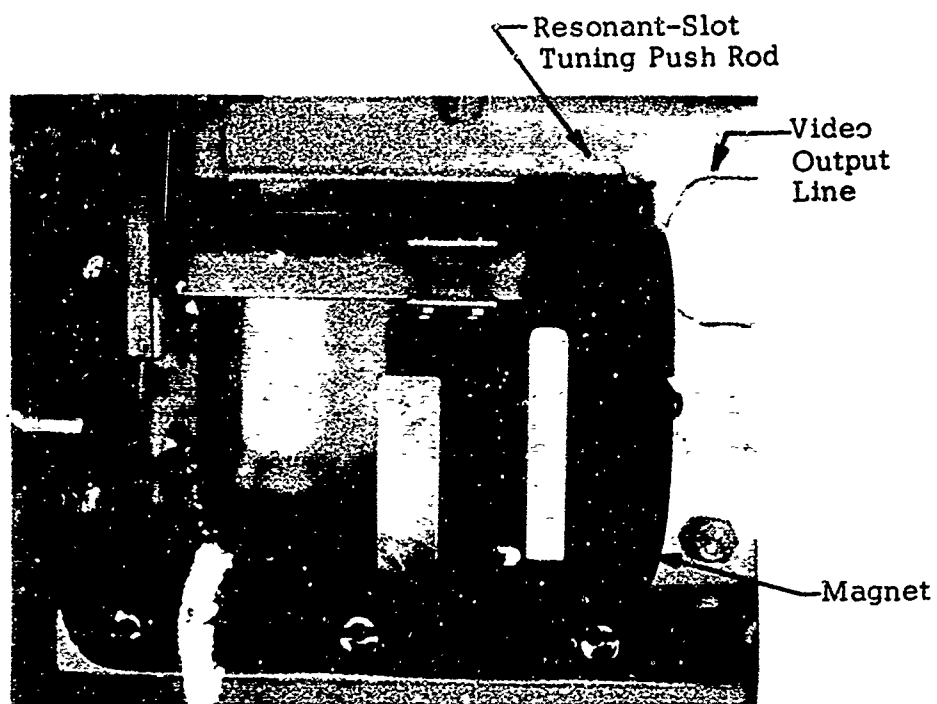


Fig. 21. Expanded view of the RF assembly and magnet shown in Fig. 2.

by means of a micrometer-type dial mechanism mounted on the front panel as shown in Fig. 18. The resonant-slot tuning push rod indicated in Fig. 21 is part of the lever arm mechanism linking the tuning dial to the rutile dielectric slab placed at the end of the pulsed-field coil resonant slot. Separate tracking of the pulse generator dc voltage for maximum RF output is required as frequency is tuned.

b. Charged-Line High-Current Pulser

The 2 ns charged-line pulser is similar to the Stanford prototype in that it consists of a pulse-forming line, a spark-gap main switch, an isolated line, a sharpening gap, and an output line. However, it differs principally in two respects:

- It has been modified to fit a standard 19-inch-wide chassis by utilizing an S-shaped microstrip line construction as shown in Fig. 22.
- It has been provided with triggering via the main spark-gap switch.

The characteristic impedance of the line is 7 ohms, with a microstrip line-width of 2 inches. Separation from the ground plane is 60 mils and consists of six sheets of 10-mil mylar insulation.

Construction of both the main spark gap and the sharpening gap also differ from the prototype. The main gap is of kovar-ceramic construction in a cylindrical configuration as shown in Fig. 22. The main gap is pressurized to 100 psig with nitrogen gas to decrease switching time of the pulse-forming line into the isolating line. Pulse rise time is decreased further through the nonlinear action of a second gap which operates at atmospheric pressure.

External adjustment of the sharpening gap in Fig. 22 is provided to optimize RF power output. The position of the sharpening gap control on the front panel is

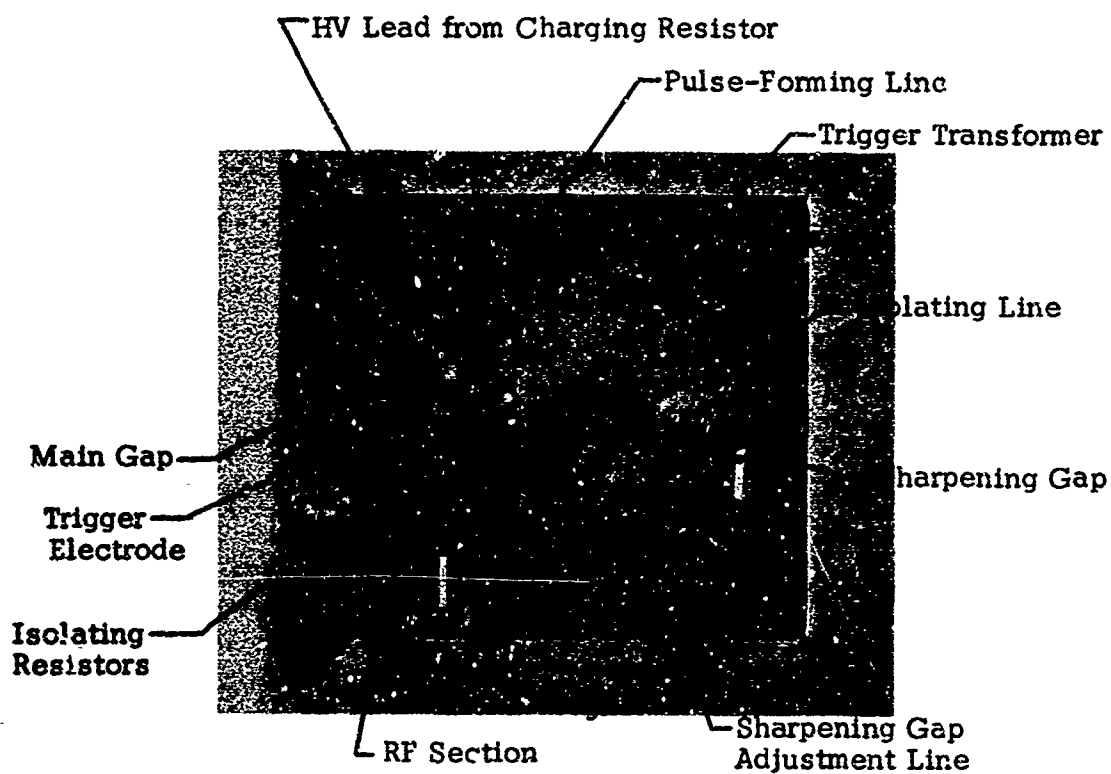


Fig. 22. Top view of the RF generator chassis showing the spark gap video pulser, the trigger transformer and the RF assembly and its magnet.

shown in Fig. 18. The correct gap adjustment is found by maximizing average RF power output as measured with a power meter connected directly to the output of the pulsed-ferrite generator.

External adjustment of the main spark gap is not provided since variation in the gap breakdown voltage (voltage to which pulse-forming line charges) required for frequency tuning is well within the dynamic range provided by the triggering described below. That is, the voltage on the pulse-forming line can be varied over a range of several kilovolts while maintaining triggered operation. The pulse current delivered to the pulsed-field coil thus varies sufficiently to operate over the frequency range of the generator without changing the main spark-gap spacing.

The bottom view of the RF generator chassis of Fig. 23 shows the placement of the 4-megohm, pulse-forming, line-charging resistor; the high voltage (18 to 25 kV) dc input connector; the nitrogen gas inlet and filter; and a high voltage connector between the charging resistor and the pulse-forming line.

c. Main Spark-Gap Triggering

Triggering of the nitrogen-pressurized main spark-gap switch is provided by means of a 50-mil diameter copper rod trigger electrode placed concentrically inside a 67-mil hole in one of the gap hemispheres. The triggering circuit is capable of PRF's in the range of 1000 to 2000 Hz. The deionization time of the main gap, however, which is pressurized to 100 psig nitrogen gas for fast pulse rise time, limits the RF generator operation to about 600 to 800 PPS. Isolation between the trigger circuit and the pulser circuit is provided by:

- placing the trigger electrode inside the main gap electrode which is connected to the isolating line between the main gap and the sharpening gap, and
- connecting a 4.9-megohm resistor to the trigger electrode in series with the trigger transformer as shown in the photo of Fig. 22 and the circuit diagram in Fig. 26.

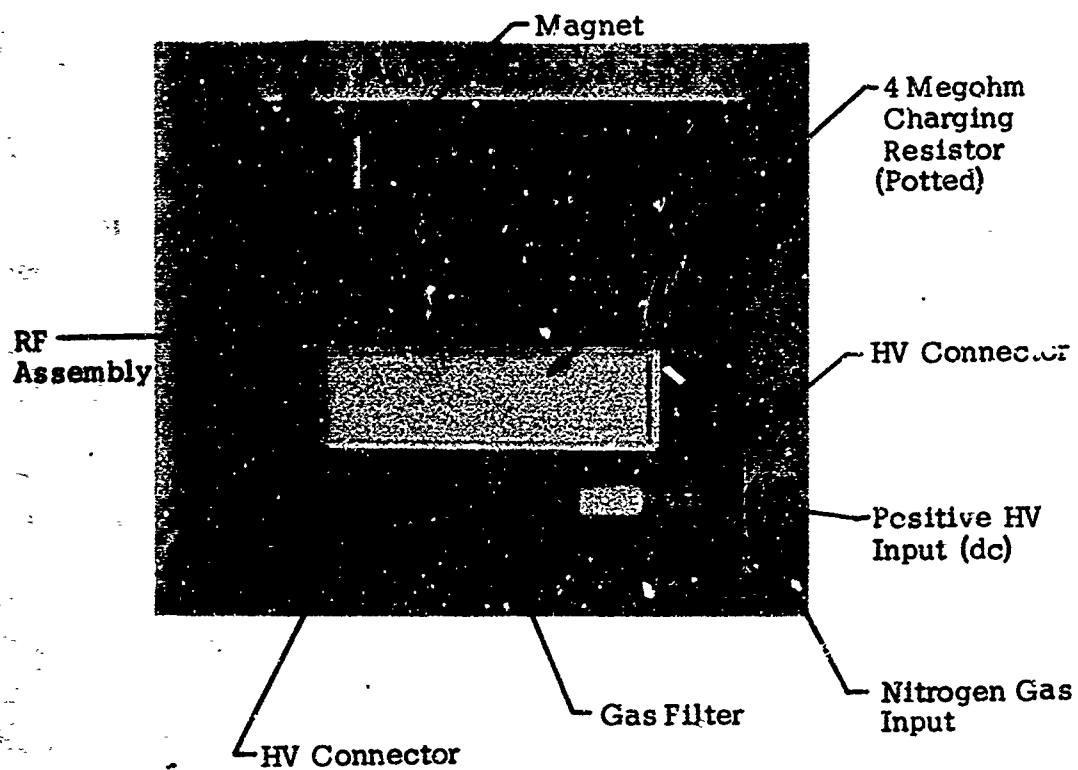


Fig. 23. Bottom view of the RF generator chassis.

This resistor limits the current supplied to the trigger gap when it fires. The value of this resistor was determined experimentally to provide maximum isolation between the trigger and pulse-forming line circuit and, at the same time, to provide efficient triggering. In this connection, it should be noted that the triggering mechanism appears to be a combination of electric field distortion and UV triggering since firing (current flow) of the trigger gap is not required to trigger the main spark gap.

The top and bottom views of the trigger generator chassis are shown in Figs. 24 and 25. They show the location of the 0 to 100 V dc power supply, the charging choke, the SCR switch, the 0.5 μ F charging capacitor, the helipot to control the power supply, and the cooling fan.

The schematic circuit diagram of the over-all X-band pulsed-ferrite generator is shown in Fig. 26. The charged-line pulser must be provided with an external 18 to 25 kV dc power supply, but sufficient space has been left in the trigger generator chassis for a 25 kV, 5 mA power supply. The trigger circuit is basically a 0.5 μ F charged-capacitor pulser, switched with an SCR switch through an ignition auto-transformer. A 0 to 100 V dc power supply with front panel control is provided for the trigger pulser. Operation at 100 V dc supplies a 15 kV trigger pulse. A standard 50-ohm pulse generator, providing a 1 to 3 μ s, 40 to 50 volt pulse, can be used to drive the SCR switch and is connected to the rear panel by a BNC connector as indicated in Fig. 19.

B. RF Test Data

Final RF test data for the X-band pulsed-ferrite generator described in the preceding section is presented in this section. This generator uses one 48-mil diameter YIG sphere. It is similar in operating principles to the Stanford prototype generator but differs in construction details. In particular, the following changes that affect the RF performance were made in the ferrite-resonant slot RF assembly.

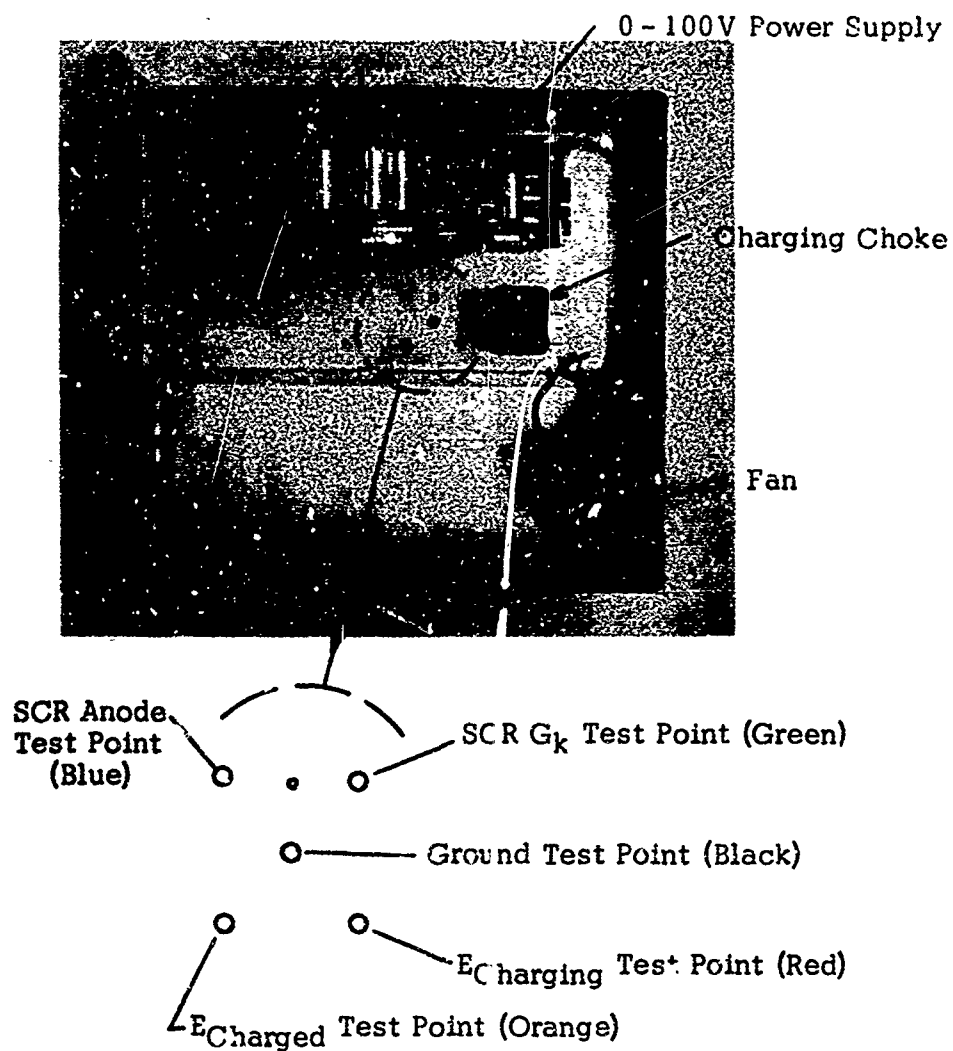


Fig. 24. Top view of the trigger chassis showing 100-volt power supply, charging choke and fan.

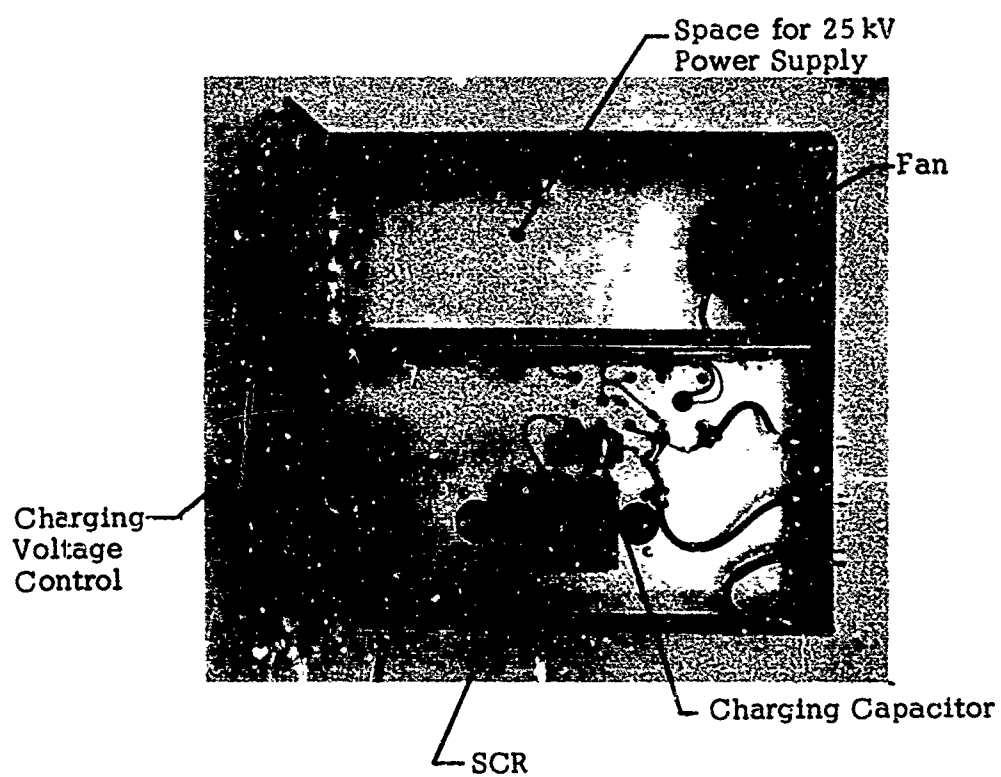


Fig. 25. Bottom view of the trigger chassis.



Fig. 26. Schematic circuit diagram of the over-all X-band pulsed-ferrite generator.

- The length of the resonant-slot in the pulsed-field coil was increased by 75 mils so that dielectric loading of the slot with Stycast dielectric loading is not required.
- The tuning mechanism has been changed mechanically so that polyfoam support material is not required inside the waveguide.

1. Q-Measurements

Because of the above changes, Q-measurements of the resonant-slot were made with a Hewlett-Packard 8410A Network Analyzer to determine Q_o , Q_L , and Q_{ext} (the unloaded, loaded and external Q's respectively). These Q values can be used to determine the energy transfer efficiency parameter, $F_{2,3}$, between the slot resonator and the waveguide, from the relationship⁽¹⁾.

$$F_{2,3} = 1 - \frac{Q_L}{Q_o} \quad (7)$$

or alternatively, since Q_o and Q_L are related by

$$Q_o = (1 + \beta) Q_L \quad (8)$$

where β is the usual cavity coupling coefficient, $F_{2,3}$ can be written as

$$F_{2,3} = \frac{\beta}{1 + \beta} \quad (9)$$

Note that β should be as large as possible since RF power output is proportional to $F_{2,3}$. That is, the optimum situation is to have an overcoupled cavity (slot) where β is much greater than unity.

The relationship of Eqn. (9) was found to be especially convenient for use with the network analyzer since β can be read directly from the Q-circle display. For the overcoupled case, that is, β is equal to the VSWR at resonance. The measured values of the energy transfer efficiency parameter, $F_{2,3}$, are plotted in Fig. 27 and compare favorably with the expected values over the frequency range of interest of 9 to 10 GHz.

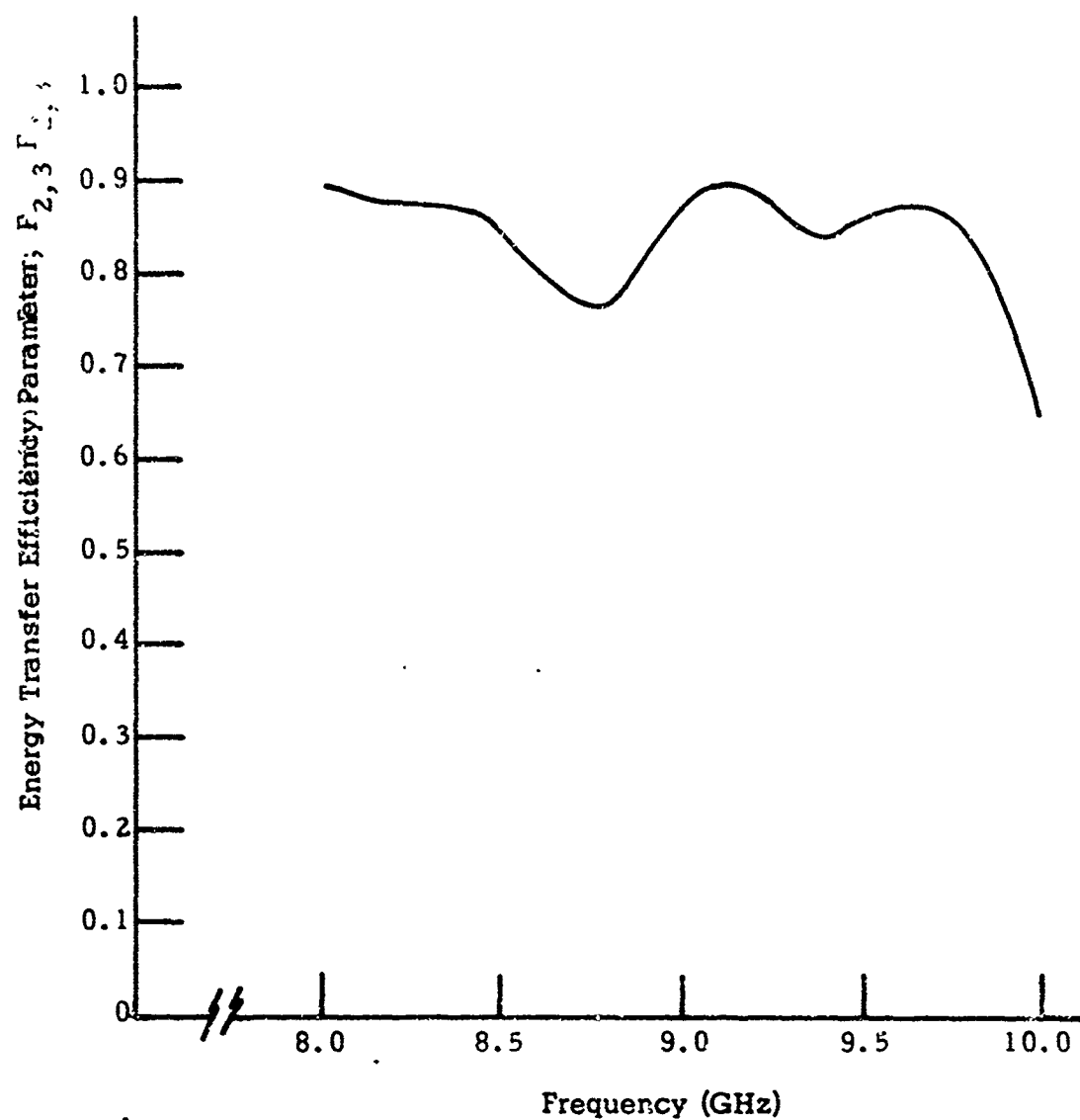


Fig. 27. Plot of the measured value of the energy transfer-efficiency parameter versus frequency.

2. Tuning

The tuning curve of the resonant slot versus the micrometer dial setting is shown in Fig. 28. This curve is measured by observing power absorption at resonance with a reflectometer. The frequency at maximum power absorption provides an indication of the output frequency of the generator.

3. RF Pulse Spectrum

The output frequency with the pulsed-ferrite RF generator in operation has also been observed with an H-P 8410B Spectrum Analyzer connected to the RF output through a 30-db attenuator. Two photos of the spectrum, with center frequency at 9.2 GHz, are shown in Fig. 29a and 29b. In Fig. 29a, the variable attenuator is set at 30 db while in Fig. 29b the setting is 20 db. The horizontal scale is 0.2 GHz/cm, so the total spectrum width is on the order of 1.8 GHz.

4. Detected RF Pulse

The corresponding detected RF pulse is shown in Fig. 30. The horizontal scale is 1 ns/cm, so the minimum pulse width is on the order of 2 ns. The equipment used for the RF pulse measurement was a Model DX164F Aertech tunnel diode having a 0.1 ns rise time, and a Tektronix Model 661 sampling scope with a 0.35 ns rise time. Note that the rise time of the detected RF is then less than 1.0 ns.

5. Charged-Line Pulser Pulse Measurement

A photo of the charged-line pulser voltage as measured on the output side of the sharpening gap is shown in Fig. 31. The pulse-forming line is charged to 20 kV. The nitrogen gas pressure is 95 psi. The horizontal scale is 1.0 ns/cm. Note that the rise time of the pulse is again on the order of 1 ns, which agrees with the rise-time measurement of the detected RF pulse. These rise-time measurements also confirm that the S-shaped microstrip charged-line pulser is performing adequately.

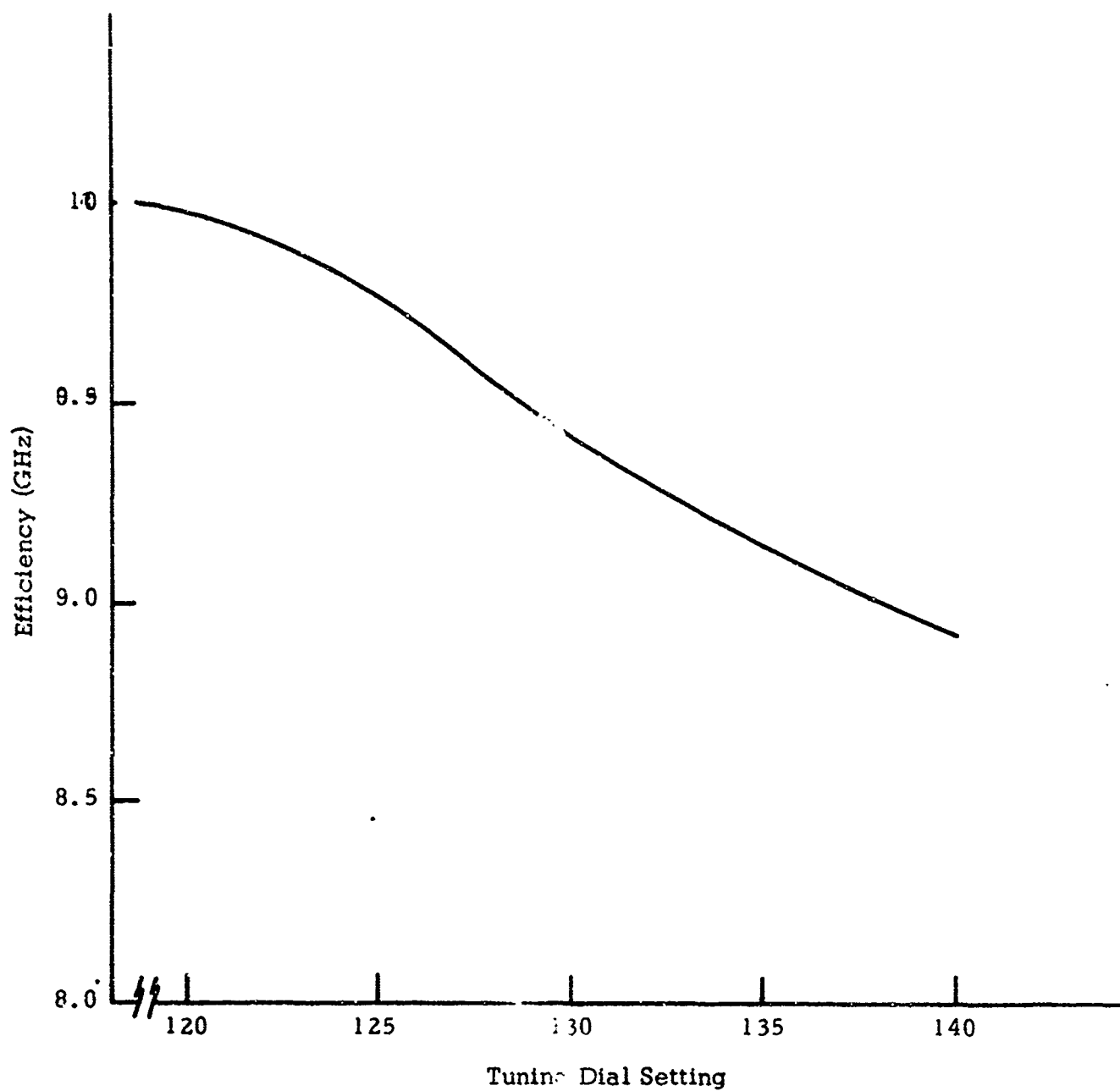
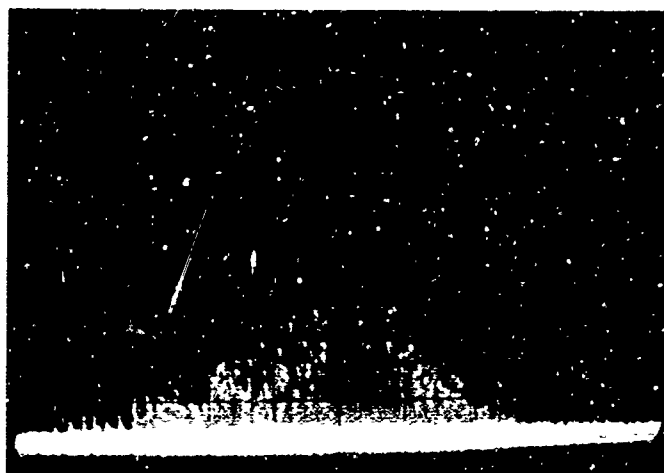


Fig. 28. Tuning curve of the resonant sl sus tuning dial setting.

(a)



(b)

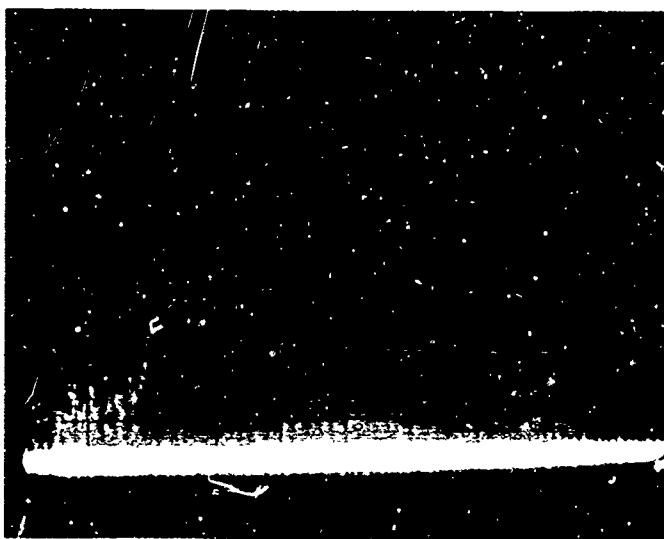


Fig. 29. Photos of the spectrum of the 2 ns pulse RF output. The horizontal scale is 0.2 GHz/cm. The center frequency is 9.2 GHz.

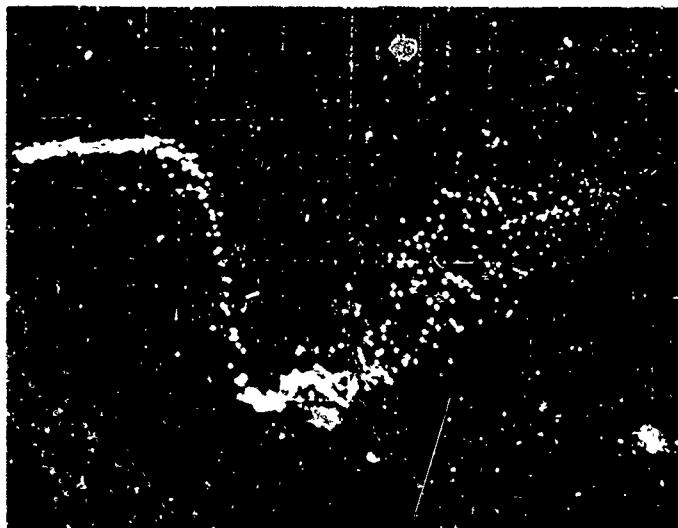


Fig. 30. Photo of the detected RF pulse as measured with 2.2 db attenuation. The horizontal scale is 1 ns/cm. The vertical scale is 50 mV/cm.

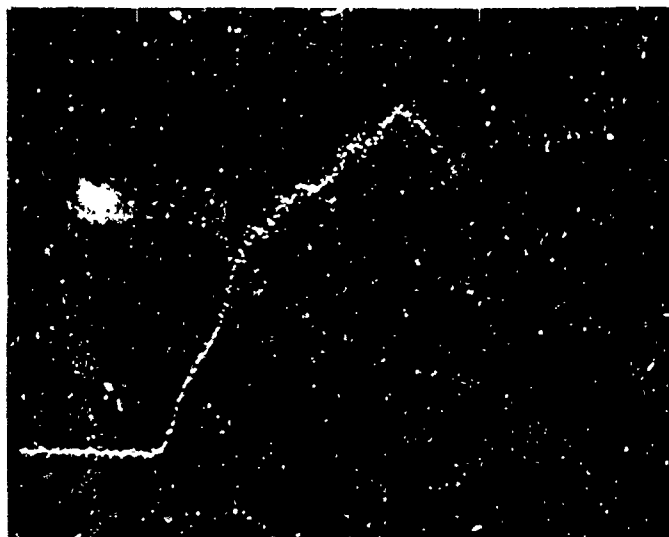


Fig. 31. Photo of the charged line pulser voltage as measured on the output side of the sharpening gap. The horizontal scale is 1.0 ns/cm. The vertical scale is 100 mV/cm after a voltage reduction factor of 11,800. The V_2 gas pressure in the main gap is 95 psig.

6. RF Power Output

The average power output of the RF generator during the measurements described above was 30 μ W at a PRF of 400 pps. The peak RF power is given by

$$\text{Peak Power} = P_{\text{avg}} / \text{Duty Cycle} = \frac{P_{\text{avg}}}{\text{PRF (pulse width)}} \quad (10)$$

For a 2.0 ns pulsewidth, therefore, and an average power of 30 μ W measured at a PRF of 400, the peak power is 37.5 watts.

The measured power is approximately 6 db below the 150-watt peak power capability of the generator as indicated by previous measurements on the prototype generator. Since the Q and pulser rise-time measurements described above indicate that the RF assembly and pulser function properly, this decrease of power output is attributed to the YIG ferrite sphere and its alignment in the resonant-slot pulsed-field coil. Optimization of power output was not completed because of failure of the 21 kV dc power supply at the end of the project shortly before the scheduled delivery of the generator. However, the optimization will be performed by the contractor required.

VI. CONCLUSIONS

Consideration of methods for increasing power output of the pulsed-ferrite generator with various multiple-sphere configurations indicates:

- Parallel arrangements of ferrites with discrete slotted-coil or vane-type coupling structures result in excessive current requirements in the pulser supplying the pulsed magnetic field.
- Series arrangements of discrete, slotted pulsed-field coils, such as used in the single-sphere generator, are subject to excessive pulse distortion which results in decreased output per sphere.
- The most feasible approach to an increase in power by an order of magnitude is to generate the required pulsed field in a uniform strip line with ferrite spheres embedded periodically in the interior of the strip line.

Coupling to the YIG spheres in the third case above is accomplished by incorporating the strip line into a waveguide-resonator-iris coupling structure. This type of multiple-sphere generator imposes severe requirements (60 kV, 1.3 kA) on the high-current nanosecond pulser supplying the required pulsed magnetic field. Work on a Darlington type of charged-line pulser for this application was performed. Pulse-to-dc charging ratios of 1.0 were achieved as compared with 0.35 for normal charged-line pulsers using spark-gap switches.

The combination of problem areas in the multiple-sphere configuration and the associated pulser requirements made incorporation of these concepts into deliverable hardware impossible within the time scale of the project.

The final X-band pulsed ferrite generator uses a single YIG resonator and has the following features:

- Triggering of the spark-gap pulser with PRFs in the range of 600 to 800 pps is provided.
- The size of the charged-line pulser has been decreased by using a folded microstrip-line construction.
- The generator is capable of delivering two-nanosecond RF pulses with one-nanosecond rise time and peak RF powers on the order of 150 watts in the X-band frequency range of 8 to 10 GHz.

A survey of the state of the art of solid-state switches to replace the spark-gap switches currently used in the charged-line pulser has been conducted. The survey indicates that although commercial thyristors (SCRs) have insufficient switching speed, this lack of speed is not due to intrinsic limitations.

VII. REFERENCES

1. H.J. Shaw, B.J. Elliott, K.J. Harker, and A. Karp, "Microwave Generation in Pulsed Ferrites", J.A.P., Vol. 37, No. 3, pp 1060-1066, March 1966.
2. E. Okress, J. Vincent, and T. Chiang, "Suppressed or Arrested Electric Discharge in Gases", Proc. IEEE, Vol. 55, No. 12, pp 2174-2175, December 1967.
3. G. Clascoc and J. Lebacqz, "Pulse Generators", pp 463-471, M.I.T. Radiation Laboratory Series, McGraw-Hill Book Company, Inc., 1948.
4. H.F. Mathis and R.F. Mathis, "Darlington Pulse-Forming Network", IEEE Trans. on Circuit Theory, pp 332-335, September 1967.
5. J.L. Moll, M. Tanenbaum, J.M. Goldey, and N. Holonyak, "P-N-P-N Transistor Switches", Proc. IRE, Vol. 44, No. 9, pp 1174-1182, September 1956.
6. F.E. Gentry, F.W. Gutzwiller, N. Holonyak, and E.E. Von Zastrow, Semiconductor Controlled Rectifiers: Principles and Applications of P-N-P-N Devices, Prentice-Hall, Inc., Englewood Cliffs, N.J., 1964.
7. R.L. Davies and James Petruzella, "P-N-P-N Charge Dynamics", Proc. IEEE, Vol. 55, No. 8, pp 1318-1330, August 1967.
8. K. Hubner and M. Melehy, "Uniform Turn-On in Four-Layer Diodes", IRE Trans. on Electron Devices, Vol. 8, No. 11, pp 461-464, November 1961.
9. "The Glass Switch", Scientific American, p. 52 (February 1968).
10. G. Sideris, "Transistors Face an Invisible Foe", Electronics, pp 191-195 (September 19, 1966).
11. J.A. Perschy, "On the Threshold of Success: Glass Semiconductor Circuits", Electronics, pp 74-84 (July 24, 1967).
12. K. M. Van Vliet, "High Injection Theories of the p-n Junction in the Charge Neutrality Approximation", Solid-State Electronics, Vol. 9, pp 185-201 (1966).

13. J.A. Hoerni and R.M. Noyce, "P-N-P-N Switches", IRE Wescon Convention Record, pp 172-175 (August 1958).
14. E.S. Yang, "Turn-Off Characteristics of P-N-P-N Devices", Solid-State Electronics, Vol. 10, pp 927-933 (1967).
15. Toshio Misawa, "Turn-On Transient of P-N-P-N Triode", Journ. Electronics and Control, Vol. 7, pp 523-533 (1959).
16. A.A. Lebedev and A.I. Uvarov, "Switching a Symmetrical P-N-P-N Structure when the Dependence of the Amplification Factors on Current is Taken into Account", Radio Engineering and Electronic Physics, No. 5, pp 830-837 (1967).
17. J.L. Moll, M. Tanerbaum, J. M. Goldey and N. Holonyak, "P-N-P-N Transistor Switches", Proc. IRE, Vol. 44, No. 9, pp 1174-1182 (September 1956).
18. A.K. Jonscher, "Notes on the Theory of Four-Layer Semiconductor Switches", Solid-State Electronics, Vol. 2, pp 1174-1182 (September 1956).
19. "Pulsed Ferrite X-Band Generator", Final Report, M.L. Report No. 1467 Microwave Laboratory, Stanford University, Stanford, California, (February 1963).

DOCUMENT CONTROL DATA - R & D

Security classification of title, body of abstract and indexing annotation must be entered when the overall report is classified

1. ORIGINATING ACTIVITY (Corporate author) MICROWAVE ELECTRONICS A Teledyne Company 3165 Porter Drive Palo Alto, California 94304		2a. REPORT SECURITY CLASSIFICATION Unclassified	
		2b. GROUP N/A	
3. REPORT TITLE PULSED MAGNETIC FIELD FERROMAGNETIC MICROWAVE GENERATOR			
4. DESCRIPTIVE NOTES (Type of report and inclusive dates) Final Progress Report			
5. AUTHOR(S) (First name, middle initial, last name) Buchmiller, L.D. Olson, F.A.			
6. REPORT DATE April 1969		7a. TOTAL NO. OF PAGES 64	7b. NO. OF REFS 19
8a. CONTRACT OR GRANT NO DAAB07-67-C-0215		8b. ORIGINATOR'S REPORT NUMBER(S)	
b. PROJECT NO 1H6-22001-A-055-05-06			
c.		9b. OTHER REPORT NO(S) (Any other numbers that may be assigned this report) ECOM-0215-F	
d.			
10. DISTRIBUTION STATEMENT This document is subject to special export controls and each transmittal to foreign governments or foreign nationals may be made only with prior approval of CG, U.S. Army Electronics Command, Ft. Monmouth, N.J. Attn: AMSEL-KL-TG			
11. SUPPLEMENTARY NOTES		12. SPONSORING MILITARY ACTIVITY U.S. Army Electronics Command Fort Monmouth, New Jersey 07703 Attn: AMSEL-KL-TG	
13. ABSTRACT <p>Engineering and packaging improvements to a prototype X-band nanosecond pulsed-ferrite generator are described. Project effort has included:</p> <ul style="list-style-type: none"> Investigations for increasing power output through the use of multiple ferrite sphere-resonator configurations, Improved charged-line spark-gap pulsers for providing pulsed magnetic fields for multiple-sphere configurations, Investigation of solid-state switch capabilities for replacing the spark-gap switches now required for switching the charged-line pulsers, Construction and testing of the final, triggered, X-band generator with a suitably compact form factor. <p>The final X-band pulsed ferrite generator uses a single YIG resonator and has the following features:</p> <ul style="list-style-type: none"> Triggering of the spark-gap pulser with PRF's in the range to 600 pps is provided, The size of the charged-line pulser has been decreased by using a folded microstrip line construction, The generator is housed in a 16 x 21 x 24-inch cabinet, The generator is capable of delivering two-nanosecond RF pulses with less than one nanosecond risetime, and peak RF powers on the order of 150 watts in the X-band frequency range of 8 to 10 GHz. 			

DD FORM 1 NOV 63 1473

(PAGE 1)

-4-

S/N 0101-807-6901

Security Classification

Security Classification

14 KEY WORDS	LINK A		LINK B		LINK C	
	ROLE	WT	ROLE	WT	ROLE	WT
<p>Ferrite Microwave Generator Nanosecond Pulses</p>						

ESC-FM 1848-69

DD FORM 1473 (BACK)
1 NOV 65
(PAGE 2)

-5-

Security Classification